

Studies of catechol-functionalized multidentate block copolymer strategy to stabilize superparamagnetic iron oxide nanoparticles for magnetic resonance imaging

Puzhen Li

A thesis in the Department of Chemistry and Biochemistry

Presented in Partial Fulfillment of the Requirements for the Degree of

Master of Science (Chemistry) at

Concordia University

Montreal, Quebec, Canada

November 2015

© Puzhen Li, 2015

CONCORDIA UNIVERSITY

School of Graduate Studies

This is to certify that the thesis prepared

By: Puzhen Li

Entitled: Studies of catechol-functionalized multidentate block copolymer strategy to stabilize superparamagnetic iron oxide nanoparticles for magnetic resonance imaging

and submitted in partial fulfillment of the requirements for the degree of

Master of Science (Chemistry)

complies with the regulations of the University and meets the accepted standards with respect to originality and quality.

Signed by the final Examining Committee:

_____ Chair

Dr. Louis Cuccia _____ Examiner

Dr. Xavier Ottenwaelder _____ Examiner

Dr. Jung Kwon (John) Oh _____ Supervisor

Approved by _____ Chair of Department or Graduate Program Director

__2015_____ Dean of Faculty

Abstract

Studies of catechol-functionalized multidentate block copolymer strategy to stabilize superparamagnetic iron oxide nanoparticles for magnetic resonance imaging

Puzhen Li

Magnetic resonance imaging (MRI) contrast agents play important roles in diagnosis and clinical applications. Particularly, superparamagnetic iron oxide nanoparticles (SNPs) with appropriate surface modification hold enormous promise as MRI contrast agents owing to their excellent biocompatibility. This thesis describes novel catechol-functionalized multidentate block copolymer (Cat-MDBC) strategy that enables the stabilization of SNPs with diameter ≤ 3.5 nm as effective MR bright imaging (T_1 -weighted) contrast agents.

Atom transfer radical polymerization and post-modification methods allow for the synthesis of well-controlled Cat-MDBC. They enable the stabilization of ultrasmall SNPs with diameter ≈ 3.5 nm (i.e. USNPs) through a biphasic ligand exchange process. The results from surface characteristics, colloidal stability in physiological properties, relaxivity properties, and *in vitro* MRI suggest that the USNPs coated with Cat-MDBC (Cat-MDBC/USNPs) can be a promising candidate for T_1 -MRI application.

Further, extremely small SNPs with diameter ≈ 2 nm (i.e. ESNPs) coated with Cat-MDBC (Cat-MDBC/ESNPs) have better relaxivity properties as T_1 -MRI contrast agents, compared with the Cat-MDBC/USNP colloids; and more promisingly, they have the r_2/r_1 value comparable to clinically-used Gd^{3+} -based contrast agents.

Acknowledgement

First, I would like to express my deepest gratitude to my supervisor, Dr. Jung Kwon Oh. It is my great fortune to have a supervisor who discovered my potential and kept encouraging me to develop and maximize it. His enormous support, sustained enthusiasm and vast knowledge helped me thrive academically and overcome the difficulties in my graduate program. I also greatly appreciate his patience and kindness in my thesis writing and revision. Without his care and edification, this thesis would have never been possible.

I would also sincerely thank my committee members Dr. Louis Cuccia and Dr. Xavier Ottenwaelder for their precious advice and giant help in my program. They have been always there to listen and give suggestions. Their advice and support help me largely improve my research and have better understanding of my projects.

My great gratitude also goes to our previous group member Dr. Nicky Chan who not only generously shared his skills and knowledge but also set a good example for me in research. Also, I feel so lucky to be able to work with Yifen, Nare, Soyoung, Depannita, Sunghwa, Kaiwan, Yasaman and all the fantastic group members in our lab. Their kindness, friendship and help made me feel like being at home even as an international student in Canada.

I also want to take this opportunity to thank our amazing collaborators: Dr. Fortin, Dr. Chevallier, Dr. Lagueux in Laval University and Dr. Vuckovich and Parsarm in Concordia University for being extremely supportive in our collaboration. I also want to show my gratitude to Dr. Gélinas, Dr. DeWolf, Dr. Rolf, Mr. Alain, Andrew, Laura and Nooshin for their kind help during my master program.

Finally, I want to thank my parents, my girl friend and my families who love and support me in every stage of my life. My love to them is beyond the word.

Contribution of Authors

Chapter 2 of this thesis is reproduced from published manuscript:

Li, Puzhen, Pascale Chevallier, Parsarm Ramrup, Depannita Biswas, Dajana Vuckovich, Marc-André Fortin, and Jung Kwon Oh. "Mussel-inspired multidentate block copolymer to stabilize ultrasmall superparamagnetic Fe₃O₄ for magnetic resonance imaging contrast enhancement and excellent colloidal stability." *Chemistry of Materials* (2015), 27, 7100-7109. DOI: 10.1021/acs.chemmater.5b03028.

Dr. Marc-André Fortin, Dr. Jean Lagueux and Pascale Chevallier in Laval University carried out the relaxivity measurements and *in vitro* MRI for Chapter 2 and 3. Dr. Dajana Vuckovich and Parsram Ramrup in Concordia University helped design and performed the colloidal stability experiment in human serum in Chapter 2. Depannita Biswas in Concordia University carried out cell viability studies for Chapter 2 and 3. Yifen Wen and Dr. Nicky Chan at Concordia University synthesized Bz-Br and TPMA for chapter 2 and 3. Alain Tessier did ICP-MS measurements for chapter 2 and 3. All other experiments were performed by the author.

Table of content

List of Figures	xi
List of Tables	xvi
List of abbreviations	xvii
Chapter 1: Introduction	1
1.1 Summary	1
1.2 MRI contrast agents.....	1
1.2.1 General background of MRI contrast agents.....	1
1.2.2 Paramagnetic contrast agents	2
1.2.3 Superparamagnetic iron oxide nanoparticles (SNPs).....	2
1.3 Surface modification of SNPs	3
1.4 Non-polymer stabilizers	4
1.4.1 Silica.....	4
1.4.2 Precious metals.....	4
1.4.3 Small molecules	5
1.5 Polymer coating.....	7
1.5.1 Dextran	7
1.5.2 Polyethylene glycol (PEG).....	8

1.5.3 Polyvinyl alcohol (PVA)	9
1.5.4 Poly(oligo (ethylene oxide) monomethyl ether methacrylate) (POEOMA) comb-polymer	10
1.6 Scope of thesis	11
Chapter 2: Mussel-inspired multidentate block copolymer to stabilize ultrasmall superparamagnetic Fe ₃ O ₄ for magnetic resonance imaging contrast enhancement and excellent colloidal stability.....	12
2.1 Introduction	14
2.2 Experimental	16
2.2.1 Instrumentation and analyses	16
2.2.2 Materials	18
2.2.3 Synthesis of POEOMA-b-PMAA (COOH-MDBC)	18
2.2.4 Synthesis of P(OEOMA-co-MAA) random copolymer (COOH-MDRC)...	19
2.2.5 Synthesis of Cat-MDBC and Cat-MDRC by coupling reaction	20
2.2.6 Biphasic ligand exchange	20
2.2.7 Conventional ligand exchange for Cat-MDRC	21
2.2.8 Cell viability using MTT assay	21
2.2.9 Colloidal stability in various pH conditions.....	22
2.2.10 Colloidal stability in human serum	22

2.2.11 Colloidal stability in the presence of protein.....	22
2.2.12 Relaxivity measurements	23
2.2.13 <i>In vitro</i> MR imaging.....	23
2.3 Results and Discussion.....	24
2.3.1 Synthesis of well-defined Cat-MDBC	24
2.3.2 Fabrication and characterization of Cat-MDBC/USNP colloids by biphasic ligand exchange	26
2.3.3 Non-cytotoxicity.....	30
2.3.4 Excellent colloidal stability in various pH and physiological conditions	31
2.3.5 Relaxometric analysis and <i>in vitro</i> T_1 -weighted MRI	33
2.3.6 Multidentate: block vs. random copolymer (Cat-MDBC vs. Cat-MDRC) ..	35
2.4 Conclusion.....	38
Chapter 3: Extremely small-sized Fe_3O_4 nanoparticles as MRI contrast agents	39
3.1 Introduction	39
3.2 Experimental	39
3.2.1 Synthesis of oleic acid stabilized ESNPs (OA-ESNPs).....	40
3.2.2 Synthesis of Cat-MDBC.....	40
3.2.3 UV-Vis spectroscopic titration.....	41
3.2.4 Colloidal stability in physiological conditions.....	42

3.3 Results and Discussion.....	42
3.4 Conclusion.....	50
Chapter 4: Conclusion and Future work.....	52
References.....	53
Appendix A.....	62
I) Synthesis and characterization of COOH-MDBC	62
II) Biphasic ligand exchange	65
III) Colloidal stability	69
IV) Colloidal stability of COOH-MDBC/USNPs	70
V) Synthesis and ligand exchange of Cat-MDRC	71
Appendix B.....	73
I) Biphasic ligand exchange.....	73
II) Calculation of UV-Vis titration	75
List of Publications	78

List of Figures

- Figure 1.1.** a) $[\text{Fe}(\text{cat})_3]^{3-}$,³³ b) $[\text{Fe}(\text{ox})_3]^{3-}$,³⁶ c) dopamine, dihydroxybenzaldehyde,³⁴ and d) dopamine-biotin conjugate.³⁵ 6
- Figure 1.2.** Scheme of the ligand exchange reaction of oleate-coated SNP with PEG-phosphate. 9
- Figure 1.3.** Molecular structure of standard linear PEG and nonlinear POEOMA constructed 10
- Figure 2.1.** Synthesis of Cat-MDBC by a facile coupling reaction of COOH-MDBC with dopamine (a) and $^1\text{H-NMR}$ spectra in DMSO- d_6 (b)..... 25
- Figure 2.2.** Schematic illustration of biphasic ligand exchange of OA-USNPs in hexane and cat-MDBC in water at the mass ratio of Cat-MDBC/USNP = 5/1 wt/wt (a), DLS diagrams (b), and TEM image (c) of aqueous Cat-MDBC/USNP colloids..... 29
- Figure 2.3.** Viability of HEK 293T and HeLa cells cultured with various concentrations of aqueous Cat-MDBC/USNP colloids at 37 °C for 48 hrs, determined by MTT assay.. 30
- Figure 2.4.** For aqueous Cat-MDBC/USNP colloids, evolution of their zeta potential over pH compared with Cat-MDBC (a), evolution of their diameter over time at various pH

= 4, 7, and 10 (b), digital images of their mixtures with human serum at 0.4 and 1.7 mg/mL (c), and no significant interaction with IgG protein (8 mg/mL) over 72 hrs determined BCA assay (d). Inset in (d) shows the digital picture of their mixtures with IgG proteins after 72 hr incubation. 33

Figure 2.5. Relaxation rates ($1/T_1$ and $1/T_2$) and T_1 -weighted MRI for aqueous Cat-MDBC/USNP colloids at 1.41 T at 37 °C. 35

Figure 2.6. For Cat-MDRC, chemical structure (a), DLS diagram (b), TEM image (c), relaxation rates ($1/T_1$ and $1/T_2$) (d), and *in vitro* MRI at 1.41T at 37 °C (e)..... 37

Figure 3.1. TEM image of OA-ESNPs (a), and Cat-MDBC/ESNP colloids (c). DLS diagrams of OA-ESNPs in hexane at 0.5 mg/mL and Cat-MDBC/ESNPs in water at 0.5 mg/mL (b). 43

Figure 3.2. Biphasic ligand exchange of OA-ESNPs in hexane and cat-MDBC in water at the mass ratio of Cat-MDBC/ESNP = 5/1 wt/wt..... 44

Figure 3.3. UV–Vis spectroscopic monitoring during titration of Cat-MDBC (a1), Cat-MDBC/ESNPs (b1). Profiles of the absorbance at 570 nm with the addition of the Fe^{3+} into Cat-MDBC (a2), Cat-MDBC/ESNPs (b2). 46

Figure 3.4. For aqueous Cat-MDBC/ESNP colloids evolution of their diameter over time in PBS at 37 °C (a), and DLS traces of Cat-MDBC/ESNPs and IgG incubated for 18 hrs and 24 hrs at 37 °C (b), Viability of HEK 293T and HeLa cells cultured with various concentrations of aqueous Cat-MDBC/ESNP colloids at 37 °C for 48 hrs, determined by MTT assay (c) and interaction of Cat-MDBC/ESNPs with IgG proteins over 24 hrs determined BCA assay (d).....	48
Figure 3.5. Relaxation rates ($1/T_1$ and $1/T_2$) and T_1 -weighted MRI for aqueous Cat-MDBC/ESNP colloids at 1.41 T at 37 °C.....	50
Figure A1. Synthetic route to COOH-MDBC by consecutive ATRP and hydrolytic cleavage.....	62
Figure A2. $^1\text{H-NMR}$ spectra of POEOMA-Br (a), POEOMA- <i>b</i> -PtBMA (b) in CDCl_3 , and POEOMA- <i>b</i> -PMAA in DMSO-d_6 (c).....	64
Figure A3. GPC traces of POEOMA-Br and POEOMA- <i>b</i> -PtBMA.....	65
Figure A4. TEM images with different magnifications of OA-USNPs.....	65
Figure A5. TGA trace of Cat-MDBC/USNP, compared with those of OA-USNPs and Cat-MDBC.....	66

Figure A6. DLS diagram and digital image (inset) of Cat-MDBC/USNP colloids in water, prepared by biphasic ligand exchange process with chloroform as an organic phase.. 67

Figure A7. DLS diagram and digital image (inset) of COOH-MDBC/USNP colloids in water, prepared by biphasic ligand exchange process with hexane as an organic phase. 68

Figure A8. DLS diagrams of aqueous Cat-MDBC/USNP colloids incubated with IgG protein (8 mg/mL) for 48 and 72 hrs. 69

Figure A9. For aqueous COOH-MDBC/USNP colloids prepared by conventional ligand exchange process, DLS diagram in aqueous solution (a), no significant interaction with IgG protein (8 mg/mL) over 72 hrs determined by BCA assay (b), digital images of their mixtures with human serum at 0.4 and 1.7 mg/mL (c), and evolution of their diameter over time at various pH = 4, 7, and 10 (d). 70

Figure A10. Synthetic route to Cat-MDRC (a) and ¹H-NMR spectra in DMSO-d₆ (b). 71

Figure A11. DLS diagram of Cat-MDRC/USNP colloids in water, prepared by conventional ligand exchange process. 72

Figure B1. TGA trace of Cat-MDBC/ESNP, compared with those of OA-ESNPs and Cat-MDBC..... 73

Figure B2. UV–Vis spectroscopic monitoring during titration of dopamine hydrochloride using Fe^{3+} (a), Profiles of the absorbance at 570 nm with the addition of the Fe^{3+} into dopamine hydrochloride (b), Multivariate fitting yielded a binding constant $\log_{10}K = 6.343 \pm 0.048$ for 1:1 model (c,d). 75

Figure B3. The molar absorptivities (ϵ in Beer-Lambert Law $A = \epsilon cl$) of Fe^{3+} , dopamineHCl their complex at different wavelength. 76

Figure B4. UV–Vis spectra overlap of the Cat-MDBC and Cat-MDBC/ESNPs before and after titration (left).Overlap of the absorbances at 570 nm with the addition of the Fe^{3+} into Cat-MDBC and Cat-MDBC/ESNPs (right)..... 76

List of Tables

Table 3.1. Size and relaxivity parameters (r_2 , r_2/r_1) of various contrast agents measured at 1.4 T	49
Table B1. Weight lose calculation based on TGA results	74

List of abbreviations

ATRP	Atom transfer radical polymerization
BCA	bicinchoninic acid
BSA	Bovine serum albumin
Bz-Br	Benzyl α -bromoisobutyrate
Cat-MDBC	Catechol functionalized multidentate block copolymer
CRP	Controlled radical polymerization
DMAP	4-(dimethylamino) pyridine
DMF	Dimethylformamide
DLS	Dynamic light scattering
EDC	1-ethyl-3-(3-dimethylaminopropyl) carbodiimide
ESNP	Extremely small iron oxide nanoparticle
FRP	Free radical polymerization
GPC	Gel permeation chromatograph
ICP-MS	Inductively coupled plasma mass spectrometry
MDBC	Multidentate dentate block copolymer
M_n	Number-average molecular weight
MTT	3-(4,5-dimethylthiazol-2-yl)-2,5-diphenyltetrazolium bromide
M_w	Weight-average molecular weight
MWCO	Molecular weight cut-off
NMR	Nuclear magnetic resonance
OA	Oleic acid
OEOMA	Oligo(ethylene oxide) methyl ether methacrylate
PMAA	Poly(methacrylic acid)
PEG	Poly(ethylene glycol)
PVA	Polyvinyl alcohol
PtBMA	Poly (tert-butyl methacrylate)
SNP	Superparamagnetic iron oxide nanoparticle
TEM	Transmission electron microscopy
TEA	Triethylamine
TFA	Trifluoroacetic acid
TPMA	Tris(2-pyridylmethyl)amine
TGA	Thermogravimetric analysis
USNP	Ultrasmall iron oxide nanoparticle
UV-Vis	Ultraviolet-Visible

Chapter 1: Introduction

1.1 Summary

The main objective of this M.Sc research is to exploit a novel multidentate block copolymer (MDBC) strategy to stabilize superparamagnetic iron oxide nanoparticles (SNPs) as effective magnetic resonance imaging (MRI) contrast agents with prolonged colloidal stability. Atom transfer radical polymerization (ATRP), a well-known controlled radical polymerization method (CRP), was employed to synthesize well-defined MDBC having pendant catechol groups that anchor to SNPs surfaces. The resultant Cat-MDBC were proved to be effective to yield aqueous Cat-MDBC/SNP colloids with hydrodynamic diameter <20 nm. The Cat-MDBC/SNPs were further characterized for colloidal stability, surface properties and magnetic properties including relaxivity and *in vitro* MRI. These results indicate that MDBC-stabilized SNPs can be promising candidates for MRI contrast enhancement.

1.2 MRI contrast agents

1.2.1 General background of MRI contrast agents

Over the last forty years since MRI was firstly reported in 1973,¹ it has become one of the most important imaging techniques in clinic use. Compared to other imaging techniques such as X-ray Computed Tomography utilizing ionizing radiation, MRI has been considered as a radiation-free imaging technique which is applicable to imaging bone and soft tissues.² In fact, the principle of MRI is similar to nuclear magnetic resonance (NMR) spectroscopy. In magnetic field under irradiation of resonant radiofrequency, the nuclei with different relaxometric properties (e.g. relaxation time) generate NMR signals with different intensities, which can be decoded into dark and bright MR images.² However to obtain high spatial resolution, the use of

MRI contrast agents is necessary.³ Paramagnetic and superparamagnetic metal ions in the contrast agents change MRI signals of tissues. Reports suggest the use of MRI contrast agents to be greater than 35% of clinical MRI scans.⁴

1.2.2 Paramagnetic contrast agents

Paramagnetic agents contain paramagnetic ions such as gadolinium (Gd^{3+}) or manganese (Mn^{2+}). The unpaired electrons in paramagnetic ions (for example, Gd^{3+} has seven unpaired electrons) can create permanent magnetic moment that can interact with small magnetic moments of the surrounding protons, usually water protons. Under the influence of this dipolar magnetic interaction, both longitudinal (T_1) and the transverse (T_2) relaxation times of these protons decrease.³ Owing to their high efficiency in decreasing proton relaxation times, Gd^{3+} -based contrast agents have been widely used for T_1 -weighted (bright) MRI.⁵ However, several concerns for Gd^{3+} -based contrast agents include their undesired bioaccumulation, toxicity and potential role in causing nephrogenic systemic fibrosis (NSF), a severe even fatal systemic disease observed in patients with history of Gadolinium-based contrast agents administration, especially those with renal diseases.⁶⁻⁸

1.2.3 Superparamagnetic iron oxide nanoparticles (SNPs)

Iron oxide nanoparticles (usually <200 nm in diameter) are presented as superparamagnetic contrast agents which contain small crystallites with several thousand magnetic ions. Superparamagnetic nanoparticles do not have permanent magnetic moment without external magnetic field, because thermal energy averages the direction of the total magnetization of the crystallite. In the presence of the external magnetic field, however, these superparamagnetic agents exhibit high saturation magnetization.⁹ Compared to paramagnetic ions, these magnetic

nanoparticles have larger magnetic moment and therefore can be effective at much lower doses (around $\mu\text{mol/kg}$ body weight).^{3, 10} SNPs are biologically tolerated and biocompatible, because iron ions generated through macrophage uptake and lysosome degradation can be incorporated into body iron store such as ferritin and hemosiderin.^{9, 11} In another aspect, since the superparamagnetic nanoparticles can be internalized into phagocytic cells like macrophages, the detection of internalized contrast agents can reveal the macrophage phagocytic activity; therefore benefiting the early diagnosis of inflammatory diseases such as atherosclerosis.¹² The fact that the superparamagnetic iron oxide agents can be designed for long circulation time also allows for the imaging of the lymphatic vessels, nodal architecture or targeted imaging.¹³

SNPs are generally designed as T_2 -contrast agents providing dark imaging in T_2 -weighted MRI. Recent advance is the development to synthesize well-defined, uniform sized, ultrasmall (diameter <10 nm) or even extremely small (diameter <3 nm) iron oxide nanoparticles (USNPs and ESNPs). The magnetic moment of iron oxide nanoparticles is proportional to their volume and thus individual particle has very small magnetic moment. (For example, the magnetic moment of ESNPs with diameter = 1.5 nm is estimated to be $3.91\mu_B$).⁹ Consequently, USNPs and ESNPs with small magnetic moment exhibit almost linear relationship between magnetization and magnetic field, which is similar to the magnetic property of paramagnetic materials.⁹ Therefore, they can be used as T_1 -contrast agents, providing bright MR imaging.

1.3 Surface modification of SNPs

Bare SNPs are easily precipitated to form aggregates due to hydrophobic interactions and magnetic attractions. Hydrophobic stabilizers such as oleic acid ($\text{C}_{18}\text{H}_{34}\text{O}_2$) are broadly used in synthesis of SNPs to control the particle size and size distribution. These hydrophobic coatings need to be changed to be hydrophilic ones for biological and biomedical applications, especially

as blood pool contrast agents. Different types of coatings or stabilizers have been designed and explored for surface modification of SNPs. In general, they can be classified as non-polymer and polymer stabilizers based on the number of repeating unit in individual stabilizer.

1.4 Non-polymer stabilizers

1.4.1 Silica

Silica coating can prevent aggregation, protect nanoparticle core and avoid the unwanted direct interaction of functional agents with SNP surfaces. Silica coatings are hydrophilic, easy for the modification with other functional groups, and have tunable thickness.^{14, 15} Stöber method enables to form in situ silica coatings through hydrolysis and condensation of sol-gel precursor. The variation of the coating thickness was achieved by changing the concentration of ammonium and the ratio of tetraethoxysilane/H₂O.^{14, 16} Microemulsion method involves the formation of microemulsions of SNPs confined in silica shells (1.8 - 30 nm).¹⁷ Although silica coating has been widely used for surface modification of nanoparticles, the lack of stability of silica in basic environments sometimes limits its use.

1.4.2 Precious metals

To protect magnetic nanoparticles from oxidation, precious metals such as gold can be used as the coating material, owing to their chemical inertness. A number of synthetic methods to synthesize precious metal coated magnetic nanoparticles have been reported, including redox transmetalation¹⁸ and microemulsion,¹⁹ which are air stable and dispersible in organic solvent or even in aqueous solution. The novel gold coated SNPs were synthesized by partial replacement reaction—use of reducing agents such as Li, Na and K to reduce FeCl₂ to form metallic core particles with diameter ≈ 11 nm, which can then reduce Au³⁺ to form gold coating with

thickness = 2.5 nm.²⁰ Further, the Au-coated magnetic nanoparticles have been explored as multifunctional contrast agents for both magnetic and dual optical applications.²¹ This can be achieved by functionalization of Au surface with thiols.²²

1.4.3 Small molecules

Small molecules functionalized with anchoring groups such as carboxylates, phosphates and catechols that can bind to the surfaces of SNPs are used as stabilizers. For the small molecules with carboxylate groups, oleic acid is the commonly-used stabilizer for the synthesis of SNPs. It allows for the synthesis of monodisperse, well-controlled SNPs and USNPs.^{23, 24} Other carboxylates include citric acid,^{25, 26} gluconic acid²⁷ and dimercaptosuccinic acid.²⁸ However these carboxylate based stabilizers exhibit a drawback that is the colloidal stabilities of SNPs stabilized with these stabilizers significantly rely on pH or ionic strength of aqueous environments.²⁹

Phosphate-based small molecules are also used to stabilize SNPs.³⁰⁻³² A report compares the properties of magnetic nanoparticles coated with different surfactants including oleic acid, lauric acid, hexadecyl phosphate, and dihexadecyl phosphate.³⁰ The results obtained for transmission electron microscope, thermogravimetric and differential scanning calorimetry measurements suggest that magnetic nanoparticles coated with carboxylate surfactants have better dispersibility in nonpolar organic solvent, while those coated with phosphate surfactants are more thermodynamically stable.³⁰

Besides carboxylates and phosphates, another type of promising anchoring group is catechol, which can form highly stable complex with iron (III) ion. As seen in Fig 1.1 the stability constant is $10^{44.9}$ of $[\text{Fe}(\text{cat})_3]^{3-}$ (octahedral complex formed by Fe^{3+} and three catechol

ligands), which is larger than that of $[\text{Fe}(\text{ox})_3]^{3-}$ (tris-oxalate complex, stability constant is $10^{18.49}$).³³ Such highly stable interaction between catechol and Fe(III) has been utilized to synthesize catechol based stabilizers for SNPs. For example, dopamine and dihydroxybenzaldehyde have been used to replace original diethylene glycol ligands on SNP surfaces to improve their colloidal stability in aqueous solution.³⁴ Biotin functionalized dopamine (Fig. 1.1d) has also been used to modify the SNP surfaces. The resulting SNPs were treated with fluorescein isothiocyanate (FITC)-labeled streptavidin, resulting in fabrication of fluorescent and magnetic responsive SNPs which are useful for protein binding, pathogen detection and molecular imaging.³⁵

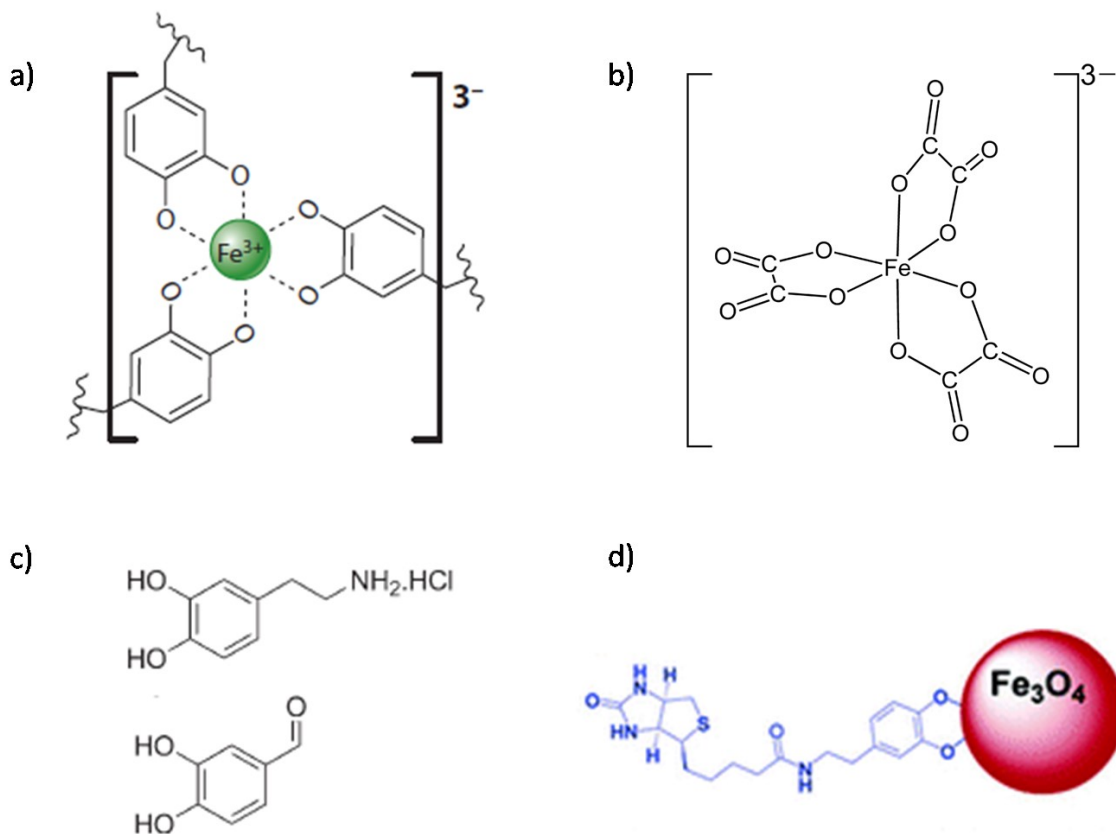


Figure 1.1. a) $[\text{Fe}(\text{cat})_3]^{3-}$,³³ b) $[\text{Fe}(\text{ox})_3]^{3-}$,³⁶ c) dopamine, dihydroxybenzaldehyde,³⁴ and d) dopamine-biotin conjugate.³⁵

1.5 Polymer coating

Apart from non-polymer stabilizers mentioned above, polymer coatings also have aroused researchers' interest world-wide, owing to their tunable size and great possibilities for further functionalization. Many polymers such as dextran,³⁷⁻⁴¹ polyethylene glycol (PEG),⁴²⁻⁴⁶ polyvinyl alcohol (PVA)⁴⁷ and poly(oligo (ethylene oxide) monomethyl ether methacrylate) (POEOMA)⁴⁸ have been synthesized and explored for magnetic nanoparticle stabilization.

1.5.1 Dextran

Dextran is a biocompatible polysaccharide with various chain lengths; thus it has been broadly used as stabilizers for commercially-available, clinically-used SNPs contrast agents such as Feridex, Resovist and Ferumoxtran-10.³⁹ Dextran coating can improve the hydrophilicity and stability of magnetic nanoparticles; it also provides prolonged blood circulation time because it decreases the non-specific interaction with plasma components.³⁷ Such prolonged blood circulation is highly desirable when contrast agents are designed for imaging for target tissues, because they could have enough time to reach the target tissues or organs.

A report describes the synthesis of dextran-coated SNPs through *in situ* coating for the formation of ferromagnetic iron-dextran particles (with diameter = 30 – 40 nm) by mixing ferrous chloride, ferric chloride and dextran (MW = 40000 g/mol) under alkaline conditions.³⁸ Further the reduction of terminal sugar moieties in dextran improve the stability of dextran-coated SNPs.⁴⁰ Another report describes the synthesis of SNPs with diameter = 5 nm by laser pyrolysis, followed by their stabilization with dextran (MW = 6000 g/mol) by sonication for 24 hrs at room temperature under basic conditions.⁴¹

1.5.2 Polyethylene glycol (PEG)

PEG is well-known to have a number of great features such as hydrophilicity, low toxicity, good biocompatibility and no immunogenicity. They are highly desirable for biological and pharmaceutical applications.⁴⁹ Thus, PEG coating can prevent aggregation of nanoparticles, improve colloidal stability in aqueous solution, and decrease the non-specific interactions with proteins or cell surfaces.⁴³ For example, PEG-phosphate (phosphate esterified PEG, Mw = 2000 or 750) has been used to replace the original oleate coating on the surface of SNPs through a process called ligand exchange as shown in the Fig. 1.2. The colloid after ligand exchange can be stable in aqueous solution at neutral or acidic pH.^{44, 45} However, in PBS or basic condition, aggregations are quickly observed, probably owing the detachment of PEG-phosphate ligands from the nanoparticles.⁴⁵ Similar design of PEG with carboxylic groups on one end was reported.⁵⁰ The stability of the nanoparticles coated with this ligand are quite limited and can only be stable in aqueous solution for one day.⁵⁰ Another type of PEG ligand design is to connect PEG to another block having multiple anchoring groups for improved colloidal stability. For example, using block copolymer polyethylene glycol-b-polyacrylic acid (PEG-b-PAA) (Mw = 5000/3200) as the coating material for nanoparticles.⁴⁶ Based on the dynamic light scattering results, the PEG-b-PAA coated nanoparticles remain stable at Tris-HCl buffer (pH = 7.4) for seven days. However, the end-group functionalized PEG precursors are usually difficult to synthesize and to separate from the unfunctionalized PEG.⁵¹

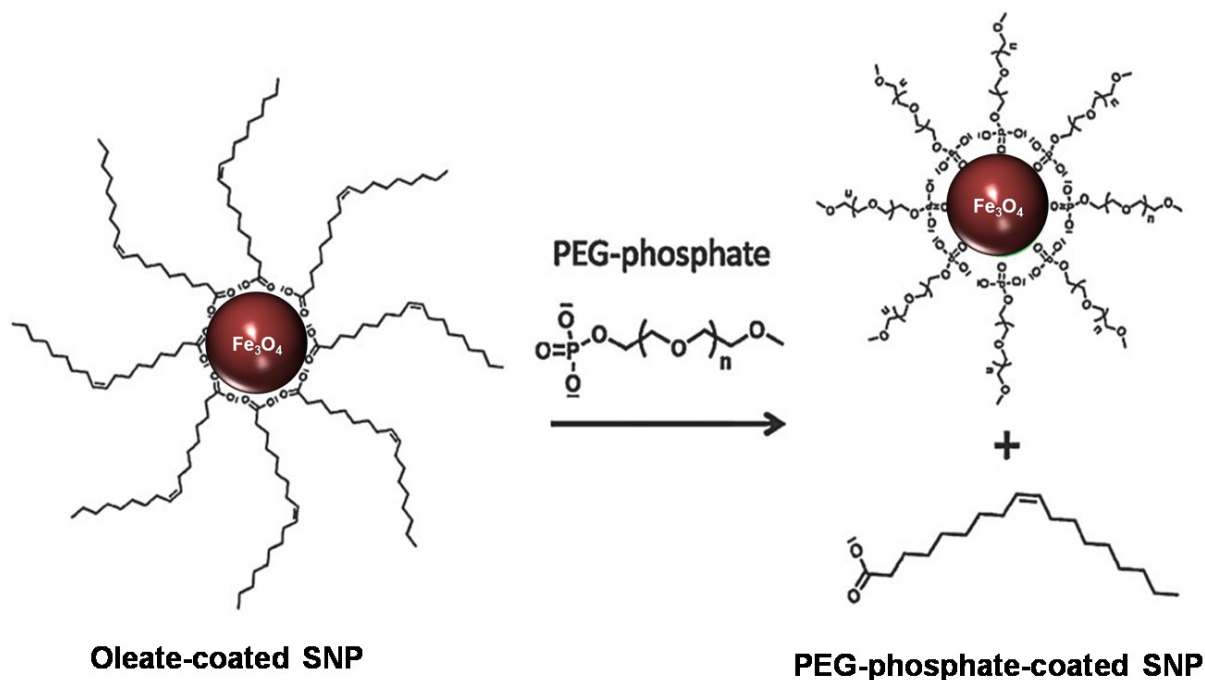


Figure 1.2. Scheme of the ligand exchange reaction of oleate-coated SNP with PEG-phosphate.

1.5.3 Polyvinyl alcohol (PVA)

Polyvinyl alcohol coatings are also explored by several research groups. For example, by directly precipitating the iron salts inside porous PVA matrices, researchers synthesized polymer-coated iron oxide nanoparticle.⁴⁷ The influences of polymer/iron mass ratio on the resulting particle sizes and colloidal stability were further studied. According to the results, the colloidal stability of PVA coated iron oxide nanoparticle at pH 7 increases with polymer ratio, probably owing to the sufficient coating of nanoparticles.⁴⁷ Other applications of PVA-stabilized iron oxide nanoparticles such as magnetic gels and magnetic films have also been reported.⁵² For example, researchers introduced ferrofluid to the PVA solution, used glutaraldehyde (GTA) as cross-linking agents to form magnetic gel, and then dry the gel to get magnetic film.⁵² They

suggested that this biocompatible, magnetic stimuli responsive film might be applied to the controlled release of drugs.⁵²

1.5.4 Poly(oligo (ethylene oxide) monomethyl ether methacrylate) (POEOMA) comb-polymer

As an analog to PEG, OEOMA monomer is biodegradable, biocompatible and hydrophilic.⁵³ Furthermore, the methacrylate moiety in OEOMA can undergo controlled radical polymerization such as atom transfer radical polymerization method (ATRP) (refer to chapter two for details) to get well-defined, narrow distributed POEOMA comb-polymers (Fig. 1.3).⁵⁴

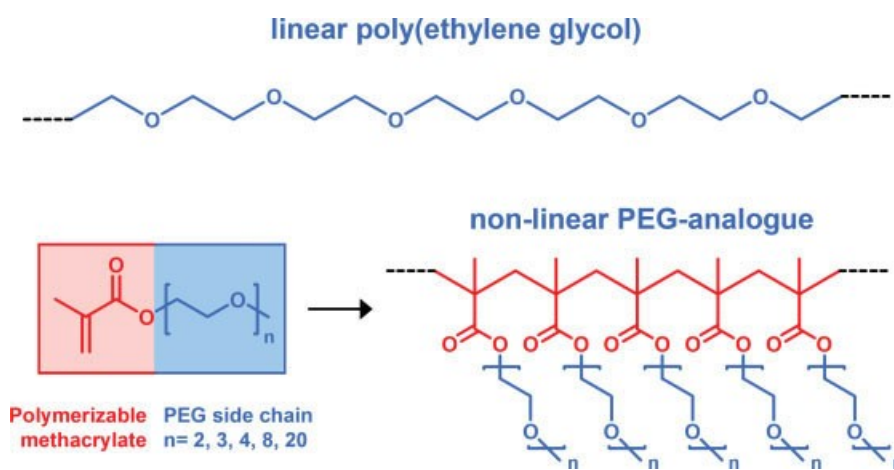


Figure 1.3. Molecular structure of standard linear PEG and nonlinear POEOMA constructed with oligo(ethylene glycol) (macro)monomers.⁵⁴

The obtained POEOMA consists of a carbon-carbon backbone and several oligo(ethylene glycol) side chains (Fig 1.3). Owing to the high portion of oligo(ethylene glycol) segments, the POEOMA polymer is water-soluble and biocompatible. Also, the maintaining halide end-functionality in POEOMA enables the consecutive ATRP to get well-controlled copolymers with different lengths, types and architectures. For example, by using two consecutive ATRP and post modification, our previous group member Dr. Nicky Chan and collaborators designed and

synthesized a multidentate block copolymer consisting of one POEOMA hydrophilic block and one poly(methacrylic acid) (PMAA) block to bind to the surface of iron oxide nanoparticles.⁴⁸ The chain lengths effect of both POEOMA and anchoring block was also explored in their following research.⁵⁵ The experimental results suggest POEOMA based multidentate block copolymer with relative long (DP >20) hydrophilic block and anchoring block can stabilize iron oxide nanoparticles under biologically relevant conditions and contribute to T_1 -weighted contrast enhancement.

1.6 Scope of thesis

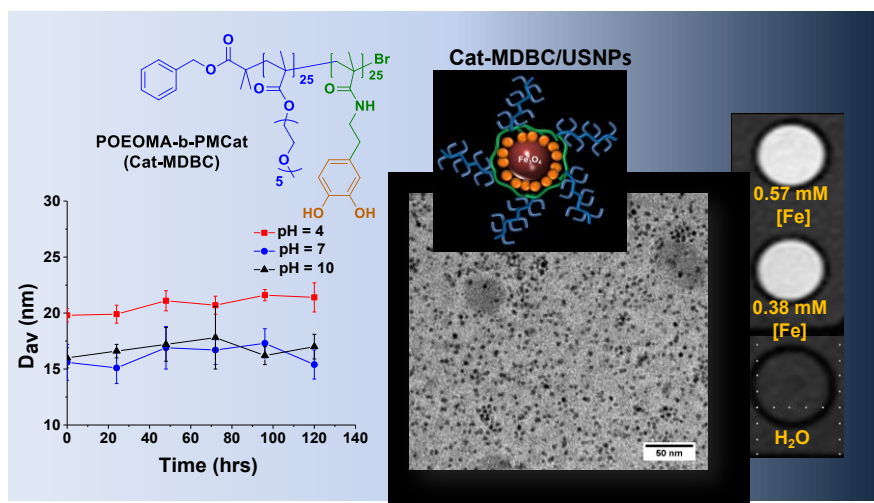
This M.Sc research project has focused on developing POEOMA based, catechol functionalized multidentate block copolymer strategy to stabilize iron oxide nanoparticles for MRI application. The research is presented in detail in the following three chapters.

Chapter 2 describes the catechol functionalized multidentate block copolymer (Cat-MDBC) stabilized 3.5 nm ultrasmall superparamagnetic Fe_3O_4 (USNPs) with magnetic resonance imaging contrast enhancement and excellent colloidal stability. Several properties of the Cat-MDBC/USNPs including colloidal stabilities, protein adsorption, relaxivity and *in vitro* MRI are evaluated.

Chapter 3 describes using similar strategy to stabilize 2 nm extremely small iron oxide nanoparticles (ESNPs). These Cat-MDBC/ESNPs are characterized and compared with Cat-MDBC/USNPs.

Chapter 4 consists of the conclusion and future work.

Chapter 2: Mussel-inspired multidentate block copolymer to stabilize ultrasmall superparamagnetic Fe₃O₄ for magnetic resonance imaging contrast enhancement and excellent colloidal stability



Colloidal ultrasmall superparamagnetic iron oxide nanoparticles (USNPs) with better control of their surface chemistry have been considered as a biocompatible alternative to clinically-used gadolinium-based contrast agents for *in vivo* bright magnetic resonance imaging (MRI). Herein, we report a versatile mussel-inspired multidentate block copolymer strategy that allows for the stabilization of USNPs as promising MRI contrast agents with excellent colloidal stability. Well-controlled multidentate block copolymer with pendant multiple catechol groups (Cat-MDBC) is synthesized by a combination of controlled radical polymerization and post-modification methods. The Cat-MDBC proves to be effective to strongly anchor to USNP surfaces as well as provide optimal hydrophilic surfaces; thus, enabling the fabrication of

aqueous Cat-MDBC/USNP colloids at single layers with diameter ≈ 20 nm through biphasic ligand exchange process. They exhibit excellent colloidal stability in broad pH range and physiological conditions; no significant protein adsorption; and great magnetic properties including relaxivity and *in vitro* MRI. Further comparison of Cat-MDBC with its corresponding catechol-based multidentate random copolymer suggests the importance of the architecture of multidentate polymeric ligands for USNP-based MRI diagnosis.

This chapter contains information that was published in *Chemistry of Materials* **2015**, 27 (20), 7100–7109 (**DOI:** 10.1021/acs.chemmater.5b03028) and part of the chapter is reproduced from the article with permission from the publisher.

2.1 Introduction

Magnetic resonance imaging (MRI) is a non-invasive imaging modality exhibiting anatomical resolution based on the stimulation of hydrogen protons by means of a precisely tuned radio frequency wave. The sensitivity and quality of MRI can be enhanced with the use of contrast agents that can induce the change in relaxation time of protons present in their immediate vicinity. In particular, colloidal superparamagnetic iron oxide nanoparticles (SNPs) are largely considered biocompatible. This is due to biodegradation and metabolism of iron oxides into iron ions which can be readily incorporated into the body's natural iron stores.⁵⁶⁻⁵⁹ SNPs are generally used as T_2 -negative contrast agents (dark image). However, the relaxivity of SNPs can be varied with their particle sizes and surface chemistry as the magnetic moment of SNPs rapidly decreases with decreasing particle size.⁶⁰⁻⁶² As such, ultrasmall SNPs (USNPs) and extremely small SNPs (ESNPs) with diameters of <5 nm have been recently explored as a biocompatible alternative to gadolinium-based T_1 -weighted contrast agents (for positive contrast enhancement).⁶³⁻⁶⁷

However, a remaining challenge to the biomedical use of SNPs including USNPs and ESNPs involves their hydrophobic surfaces that have to be modified to hydrophilic ones; thus they can be colloidally stable as well as compatible with biological environments.^{68, 69} One main approach is the ligand exchange process where hydrophobic ligands that originally bound to their surfaces such as oleic acids are replaced with hydrophilic ones that possess anchoring groups such as carboxylic acids, phosphates, and amines.^{70, 71} Polymers possessing multiple anchoring groups capable of multiple binding interactions with SNP surfaces have been designed as effective multidentate ligands.⁷²⁻⁷⁴ In particular, multidentate block copolymers (MDBC)s consist of one block possessing pendant multidentate anchoring groups strongly bound to SNP

surfaces, allowing for the fabrication of aqueous colloidal SNPs with single ligand layers. The other hydrophilic block can promote compatibility with biological environments. Recent reports have proved that the MDBC stabilization having pendant carboxylates and phosphonates as anchoring groups is an effective strategy enabling the fabrication of colloidally-stable SNPs in aqueous solutions as effective MRI contrast agents.^{48, 55, 75-78} Our group has also reported the synthesis and conventional ligand exchange of well-controlled MDBC having pendant carboxylic acids in the anchoring block and oligo(ethylene oxide) groups in the hydrophilic block (COOH-MDBC).⁴⁸ The resultant USNPs stabilized with COOH-MDBC having longer block lengths exhibit enhanced colloidal stability in physiological conditions as well as *in vitro* and *in vivo* T_1 -weighted contrast enhancement.⁵⁵ However, one concern for carboxylated MDBC-coated USNPs involves their negatively-charged surfaces (zeta potential, $\zeta \approx -10$ mV at pH = 7). The design of neutral surfaces could be desirable to minimize protein absorption, thus providing prolonged blood circulation and enhancing MRI contrast enhancement.

Inspired by mussels, catechol-based ligands have been utilized as high-affinity anchors.^{79, 80} However, most ligands possess one catechol binding units as small molecules, oligomers, or macromolecules;⁸¹⁻⁸⁶ such monodentates impart poor stabilities because of a constant equilibrium of adsorption/desorption from the particle surface, eventually causing precipitation due to the loss of colloidal stability. Further, catechol-functionalized polymeric multidentates as homopolymers,⁸⁷ random copolymers,⁸⁸⁻⁹⁰ and branched polymers⁹¹ have been synthesized. However, no reports have described the use of block copolymer-based multidentates having pendant multiple catechol groups for the surface modification of SNPs and USNPs yet.

In this study, we have explored a mussel-inspired multidentate block copolymer strategy to stabilize USNPs as an effective T_1 -positive contrast agent with excellent colloidal stability in

various pH and physiological conditions. A combination of controlled radical polymerization, hydrolytic cleavage, and facile coupling reaction was employed to synthesize well-defined MDBC having pendant catechol groups in the anchoring block and oligo(ethylene oxide) groups in the hydrophilic block (Cat-MDBC). Compared with catechol-containing homopolymers, the presence of oligo(ethylene oxide) in Cat-MDBCs could provide hydrophilic sheath property during blood circulation *in vivo*, similar to poly(ethylene oxide), an analog of oligo(ethylene oxide).⁹²⁻⁹⁴ The resultant Cat-MDBC was examined to be effective for a heterogeneous ligand exchange process on USNP surfaces, replacing originally-stabilizing monodentates (i.e. oleic acid) in an organic layer. This process can allow for fabrication of USNPs stabilized with Cat-MDBC in aqueous solution, thus forming aqueous Cat-MDBC/USNP colloids with single layers. The resulting aqueous Cat-MDBC/USNP colloids were evaluated as effective T_1 contrast agents for excellent colloidal stability in various pH and physiological conditions, in the presence of proteins, and in serum as well as for magnetic properties using relaxometry and *in vitro* MRI at clinical magnetic field strengths. Further, Cat-MDBC was compared with the counterpart of multidentate random copolymer having pendant catechol groups (Cat-MDRC) for their effectiveness in MRI.

2.2 Experimental

2.2.1 Instrumentation and analyses

¹H-NMR spectra were recorded using a 500 MHz Varian spectrometer. CDCl₃ singlet at 7.26 ppm or DMSO-d₆ quintet at 2.50 ppm was selected as the reference standard. Monomer conversion was determined using ¹H-NMR. Molecular weight and molecular weight distribution were determined by gel permeation chromatography (GPC) on an Agilent GPC equipped with a

1260 Infinity Isocratic Pump and a RI detector was used. Two Agilent PLgel mixed-C and mixed-D columns were used with DMF containing 0.1 mol% LiBr at 30 °C at a flow rate of 1.0 mL/min. Linear poly(methyl methacrylate) standards from Fluka were used for calibration. Aliquots of polymer samples were dissolved in DMF. The clear polymer solutions were filtered using a 0.2 µm PTFE filter to remove any solvent-insoluble species. A drop of anisole was added as a flow rate marker.

Zeta potential (ζ) for aqueous Cat-MDBC/USNP colloids and Cat-MDBC at different pH values were measured using Zeta Potential Analyzer (Brookhaven) in 10 mM aqueous NaCl solution at 25 °C. The pH values were adjusted using 50 mM aqueous HCl and 50 mM aqueous NaOH solutions.

Transmission Electron Microscopy (TEM) images were taken using a Philips Tecnai 12 TEM, operated at 120 kV and equipped with a thermionic LaB6 filament. An AMT V601 DVC camera with point to point resolution and line resolution of 0.34 nm and 0.20 nm respectively was used to capture images at 2048 by 2048 pixels. To prepare specimens, USNPs stabilized with OAs and Cat-MDBCs in organic and aqueous solutions was dropped onto copper TEM grids (400 mesh, carbon coated) and then allowed to air dry at room temperature.

Dynamic light scattering (DLS) was used to determine hydrodynamic diameters by volume of USNPs stabilized with OAs and copolymers in organic and aqueous solutions at a fixed scattering angle of 175° at 25 °C with a Malvern Instruments Nano S ZEN1600 equipped with a 633 nm He-Ne gas laser.

Thermogravimetric analysis (TGA) measurements were carried out using a TA instruments Q50 analyzer. Typically, the dialyzed, freeze dried samples (5-10 mg) were placed into a

platinum pan and heated from 25 to 800 °C at a heating rate of 20 °C/min under nitrogen flow. The mass loss between 250 and 600 °C was used to calculate the USNP content in Cat-MDBC/USNPs.

2.2.2 Materials

Benzyl alcohol (99%), triethylamine (Et₃N, >99.99%), copper(II) bromide (CuBr₂, >99.99%), tin(II) 2-ethylhexanoate (Sn(EH)₂, 95%), trifluoroacetic acid (TFA, 99%), iron(II) chloride (FeCl₂, 98%), iron(III) chloride (FeCl₃, 97%), oleic acid (OA, 97%), dopamine hydrochloride, 4-(dimethylamino)pyridine (DMAP, >99.99%), 1-ethyl-3-(3-dimethylaminopropyl) carbodiimide (EDC, >98%), immunoglobulin G from human serum (IgG, reagent grade, ≥95%, essentially salt-free, lyophilized powder) and human serum (male, AB type) from Sigma Aldrich as well as Pierce BCA protein assay kit was from Bio-Rad were used as received. Oligo(ethylene oxide) methyl ether methacrylate (OEOMA) with MW = 300 g/mol and pendant EO# ≈ 5 and tert-butyl methacrylate (tBMA) from Aldrich were purified by passing through a column filled with basic alumina to remove inhibitors before use. Tris(2-pyridylmethyl)amine (TPMA),⁹⁵ benzyl α-bromoisobutyrate (Bz-Br),⁹⁶ and OA-stabilized USNPs (OA-USNPs)⁴⁸ were synthesized as described in our previous publications.

2.2.3 Synthesis of POEOMA-b-PMAA (COOH-MDBC)

The detailed synthesis by ATRP is described in appendix A. Molecular weight: $M_n = 7,800$ g/mol and $M_w/M_n = 1.24$ for POEOMA-Br and $M_n = 9,300$ g/mol and $M_w/M_n = 1.24$ for POEOMA-b-PtBMA.

2.2.4 Synthesis of P(OEOMA-co-MAA) random copolymer (COOH-MDRC)

Similar to COOH-MDBC, two steps were designed. The first step is ATRP of OEOMA and tBMA in the presence of Bz-Br with the initial mole ratio of $[\text{OEOMA}]_0/[\text{tBMA}]_0/[\text{Bz-Br}]_0 = 70/70/1.0$. Bz-Br (0.1 g, 0.38 mmol), OEOMA (7.9 g, 26.4 mol), tBMA (3.76 g, 26.4 mmol), CuBr_2 (4.2 mg, 18.7 μmol), TPMA (16.3 mg, 56 μmol), and anisole (24 g) were mixed in a 50 mL Schlenk flask. The mixture was deoxygenated by purging under nitrogen for 1 hr, and then placed in an oil bath at 40 °C. A nitrogen pre-purged solution of $\text{Sn}(\text{EH})_2$ (61.2 mg, 151 μmol) dissolved in anisole (0.5 g) was injected into the Schlenk flask to initiate polymerization. Polymerization was stopped after 3 hrs by cooling the reaction mixture in an ice bath and exposing it to air.

For purification, the as-synthesized polymer solution was precipitated from cold hexane three times to remove unreacted monomers. The precipitates were dissolved in acetone and then passed through a column filled with basic alumina to remove residual copper species. The polymer solution was passed through a 0.2 μm PTFE filter to remove residual tin species. The product of P(OEOMA-co-tBMA) was isolated by removal of solvents by rotary evaporation and further drying in a vacuum oven at room temperature for 24 hrs. Molecular weight: $M_n = 11,900$ g/mol and $M_w/M_n = 1.18$.

The next step is the hydrolytic cleavage of P(OEOMA-co-tBMA). The purified, dried P(OEOMA-co-tBMA) (0.4 g, 56.5 μmol) dissolved in dichloromethane (8 mL) was mixed with TFA (10 fold excess to the mole of pendant t-butoxy groups) under stirring for 24 hrs. The resulting mixtures were concentrated using rotary evaporation and precipitated from cold hexane

three times. The precipitates were then dried in a vacuum oven at room temperature for 24 hrs to form COOH-MDRC.

2.2.5 Synthesis of Cat-MDBC and Cat-MDRC by coupling reaction

A EDC coupling reaction was used with the initial mole ratio of $[\text{COOH}]_0/[\text{dopamine}]_0/[\text{EDC}]_0/[\text{Et}_3\text{N}]_0/[\text{DMAP}]_0 = 1/4/1.1/5.5/0.1$. Typically, an organic solution consisting of the purified, dried COOH-MDBC (0.2 g, COOH = 0.5 mmol calculated with the DP of PMAA block), EDC (82 mg, 0.53 mmol), Et₃N (54 mg, 0.53 mmol), and DMF (5 mL) was mixed with an organic solution consisting of Et₃N, (215 mg, 2.13 mmol), dopamine hydrogen chloride salt (366 mg, 1.93 mmol), DMAP (7 mg, 0.06 mmol), and DMF (5 mL). The mixture was stirred at 80 °C in an oil bath for 2 days. The solution turned brown. The reaction mixture was purified by vacuum filtration, followed by intensive dialysis using a dialysis tubing with MWCO = 3.5 kDa over water for 3 days. The purified MDBC were lyophilized. Similar procedure was used for Cat-MDRC.

2.2.6 Biphasic ligand exchange

For the preparation of aqueous Cat-MDBC/USNP colloids, aliquots of a stock solution of OA-USNPs in hexane (0.4 mg/mL, 5 mL) were mixed with aliquots of aqueous stock solution of Cat-MDBC (2 mg/mL, 5 mL). The resulting biphasic mixtures were sonicated using a digital sonifier (Branson) for 40 min at 30% amplification. After sonication, the bottom aqueous layer was collected, filtered through 0.45 μm PES filter, and then purified by an intensive dialysis using a tubing with MWCO = 25 kDa over deionized water (2 L) for 3 days. The resulting dispersions were lyophilized using a freeze drier. The purified, lyophilized Cat-MDBC/USNPs

could be re-dispersed in water by stirring or sonication. The similar procedure was examined for Cat-MDRC and COOH-MDBC.

2.2.7 Conventional ligand exchange for Cat-MDRC

Aliquots of the purified, dried Cat-MDRC (10 mg) were mixed with aliquot of the purified OA-USNPs (2 mg) in a mixture of 2/1 v/v chloroform/EtOH (5 mL) under magnetic stirring at room temperature for 24 hrs. The resulting mixture was precipitated from hexane, and then centrifuged at 5,000 rpm for 10 min. The resulting brown pellet was re-dissolved in chloroform and the similar procedure was repeated three times to remove unbound OA species. The centrifuged pellet was dried in a vacuum oven at room temperature to yield Cat-MDRC/USNPs. After ligand exchange, aliquots of Cat-MDRC/USNPs were dispersed in water and dialyzed using a dialysis tubing with MWCO = 25 kDa over water (2 L) for 3 days. After dialysis, the purified Cat-MDRC/USNPs were lyophilized using a freeze drier. The similar procedure was examined for COOH-MDBC.

2.2.8 Cell viability using MTT assay

Human embryonic kidney (HEK 293T) and HeLa cancer cells were cultured in DMEM (Dulbecco's modified Eagle's medium) containing 10% FBS (fetal bovine serum) and 1% antibiotics (50 units/mL penicillin and 50 units/mL streptomycin) at 37 °C in a humidified atmosphere containing 5% CO₂. Cells were plated at 5 x 10⁵ cells/well into a 96-well plate and then incubated with various concentrations of Cat-MDBC/USNP colloids for 48 hrs. Blank controls (cells only) were run simultaneously. Cell viability was measured using CellTiter 96 Non-Radioactive Cell Proliferation Assay kit (MTT, Promega) according to manufacturer's instruction. Briefly, 3-(4,5-dimethylthiazol-2-yl)-2,5-diphenyltetrazolium bromide (MTT)

solutions (15 μL) was added into each well. After 4 h incubation, the medium containing unreacted MTT was carefully removed. DMSO (100 μL) was added into each well in order to dissolve the formed formazan blue crystals, and then the absorbance at $\lambda = 570 \text{ nm}$ was recorded using Powerwave HT Microplate Reader (Bio-Tek). Each concentration was 12-replicated. Cell viability was calculated as the percent ratio of absorbance of mixtures with colloids to control (cells only).

2.2.9 Colloidal stability in various pH conditions

Aliquots of aqueous Cat-MDBC/USNP dispersion at 0.2 mg/mL were mixed with the equal volumes of buffer solutions at different pHs: an aqueous mixture of 0.1 M NaOH (0.1 mL) and 0.1 M potassium hydrogen phthalate (50 mL) for pH = 4.0 buffer, a commercially-available PBS for pH = 7.4, and an aqueous mixture of 0.1 M NaOH (11 mL) and 0.05 M NaHCO_3 (50 mL) for pH = 9.8.

2.2.10 Colloidal stability in human serum

Aliquots of 150 mM saline aqueous Cat-MDBC/USNP dispersion (5 mg/mL) were mixed with different volumes of a human serum to adjust the concentration of Cat-MDBC/USNP to be 0.4 and 1.7 mg/mL. Colloidal stability was followed by naked eyes over times.

2.2.11 Colloidal stability in the presence of protein

Stock solutions of Cat-MDBC/USNPs at 1.2 mg/mL and human IgG at 8 mg/mL were prepared in PBS (pH = 7.4). They were mixed and incubated at 37 $^{\circ}\text{C}$. Aliquots were taken at 48 and 72 hrs and subjected to centrifugation (18,000 rpm, 4 $^{\circ}\text{C}$, 30 min) in attempt to precipitate undesirably-formed aggregates. The concentration of IgG protein in supernatant before and after

centrifugation was measured using Pierce BCA protein assay kit at $\lambda = 562$ nm wavelength and compared with that of IgG protein (no Cat-MDBC/USNP) as a control.

2.2.12 Relaxivity measurements

Aqueous Cat-MDBC/USNPs dispersion at 1.0 mg/mL was prepared using the similar protocol as described above. After aliquots of the dispersion were diluted with different volumes of water, the resulting dispersions were dispensed into 7.5 mm o.d. NMR tubes. Their longitudinal and transversal relaxation times (T_1 and T_2) were measured with a dedicated TD-NMR relaxometer (Bruker Minispec 60 mq, 60 MHz (1.41 T, 37 °C). For the measurement of T_1 , a standard inversion-recovery sequence was used (180° inversion pulse, followed by a certain delay (TI), then a 90° pulse to measure the intensity of the free induction decay signal). After a recovery period of at least 3 seconds, the sequence was repeated with a different delay (TI). The T_1 curve was drawn using points acquired from at least 15 different delays. For T_2 measurements, a standard Carr-Purcell-Meibom-Gill sequence was used (90° pulse, followed by 180° rephasing pulses to induce the echo; the T_2 curve was drawn from measurements performed on at least 12 echos). The Fe content in the dispersions was precisely determined by Inductively-Coupled Plasma Mass spectrometry (ICP-MS; Agilent 7500ce). Prior to ICP measurements, aliquots of each Cat-MDBC/USNP and Cat-MDRC/USNP dispersion (≈ 0.1 mg/mL) were digested overnight at 80 °C in HNO₃ (trace metal, Fisher Scientific A509–500) and 30% H₂O₂ (Sigma-Aldrich).

2.2.13 *In vitro* MR imaging

Aliquots of Cat-MDBC/USNP and Cat-MDRC/USNP colloids were dispensed into 500 μ L polyethylene centrifugation tubes. The tubes were immersed in water, inserted in a 60-mm RF coil and imaged at 25 °C with a 1T small-animal MRI system (M2M, Aspect Imaging, Israel). A

T_1 -weighted 2D spin-echo sequence was used as follows: TE = 10.8 ms; TR = 400 ms; $\alpha = 90^\circ$; FOV = 70 mm; 1.4 mm slices with 0.1 mm gap; dwell time = 16 μ s; matrix: 200 \times 200; 3 exc. A T_2 -weighted 2D spin-echo sequence was also used: TE = 75 ms; TR = 2500 ms; $\alpha = 90^\circ$; FOV = 70 mm; 1.4 mm slices with 0.1 mm gap; dwell time = 16 μ s, matrix: 200 \times 200; 1 exc.

2.3 Results and Discussion

2.3.1 Synthesis of well-defined Cat-MDBC

As illustrated in Figure 2.1a, well-controlled Cat-MDBC block copolymer (i.e. POEOMA-*b*-PMCat) was synthesized by a facile carbodiimide-mediated coupling reaction of pendant COOH groups of COOH-MDBC (i.e. POEOMA-*b*-PMAA) with amino groups of dopamine. As described,⁸⁸ the products were purified by an intensive dialysis to remove byproducts and unreacted precursors. $^1\text{H-NMR}$ spectroscopy was used to follow the coupling reaction (Figure 2.1b). $^1\text{H-NMR}$ of Cat-MDBC shows the presence of pendant catechol groups at 6.3-6.7 ppm (e), pendant OEO moieties at 4.0 ppm (b) and 3.2-3.7 ppm, backbone methyl groups at 0.7-1.1 ppm (c, d), and terminal phenyl groups at 7.3 ppm (a). Using the integral ratio of the peaks (b, c, d, and e), the extent of coupling reaction was determined to be >90 %. This result suggests the successful synthesis of Cat-MDBC having pendant catechol groups.

The precursor, COOH-MDBC, was synthesized as described in our previous publication.⁴⁸ As illustrated in Figure A1 in appendix A, the first step is the consecutive atom transfer radical polymerization (ATRP),^{97, 98} yielding well-controlled POEOMA₂₅-*b*-PtBMA₂₅ with the degree of polymerization (DP) = 25 for both POEOMA and PtBMA blocks. The second step is the hydrolytic cleavage of pendant *t*-butoxy groups of PtBMA block to the corresponding

POEOMA-b-PMAA (COOH-MDBC). The detailed synthesis and characterization by $^1\text{H-NMR}$ for composition and GPC for molecular weight are described in appendix A (Figure A2 and A3).

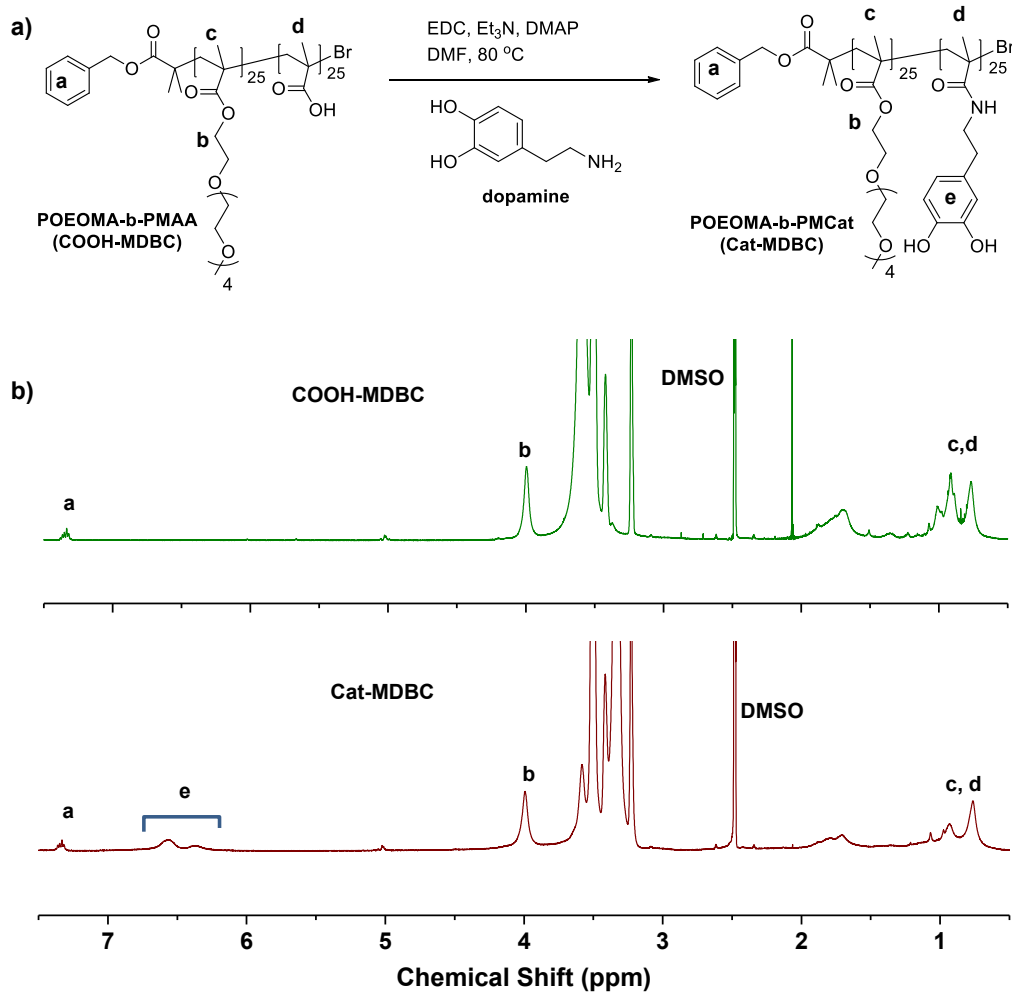


Figure 2.1. Synthesis of Cat-MDBC by a facile coupling reaction of COOH-MDBC with dopamine (a) and $^1\text{H-NMR}$ spectra in DMSO-d₆ (b).

2.3.2 Fabrication and characterization of Cat-MDBC/USNP colloids by biphasic ligand exchange

Colloidal USNPs stabilized with oleic acid (OA-USNPs) was synthesized by co-precipitation of Fe(II) and Fe(III) in a water/toluene/ethanol mixture. The purified OA-USNPs had a diameter = 10 nm in hexane (1 mg/mL) by DLS and core diameter = 3.5 ± 1.1 nm by TEM (Figure A4). To fabricate colloidal USNPs stabilized with Cat-MDBC in aqueous solution (aqueous Cat-MDBC/USNP colloids), a biphasic ligand exchange method reported in literature⁹⁹ was exploited (Figure 2.2a). An aqueous Cat-MDBC solution in water (2 mg/mL) was mixed with an organic OA-USNP solution in hexane (0.4 mg/mL) in the equal volumes at the mass ratio of Cat-MDBC/OA-USNP = 5/1. The resulting biphasic mixture was then subjected to sonication for 40 min and allowed for phase separation at room temperature for 12 hrs. The aqueous bottom layer was then carefully decanted and then dialyzed using a dialysis tubing (MWCO = 25 kDa) against water in an attempt to remove free (not bound) copolymers, yielding a black-colored dispersion at 0.8 mg/mL concentration (III in Figure 2.2a). The resulting dispersion was then lyophilized using a freeze-drying method. The dried Cat-MDBC/USNPs were readily re-dispersed in aqueous solution by a simple magnetic stirring at various concentrations (IV in Figure 2.2a).

During the ligand exchange process, pendant catechol groups in the copolymer block are anchored to USNP surfaces. Such enhanced binding isotherm enables the formation of individual USNPs at a single layer of Cat-MDBC. However, it could also result in the formation of undesired large-sized agglomerates or clusters composed of several individual USNPs anchored by multiple catechol groups of individual MDBC chains. Considering the core diameter of USNPs and the size of Cat-MDBC in water, the agglomerates could have their diameters greater

than approximately 35 nm. Here, DLS result indicates the hydrodynamic diameter of colloidal Cat-MDBC/USNP to be ≈ 20 nm with monomodal and narrow size distribution in aqueous solution (Figure 2.2b). Further DLS analysis suggests the presence of agglomerates (with diameter >35 nm) to be $<15\%$. TEM image of Cat-MDBC/USNP colloids shows mostly individually-distinct USNPs with a small population of aggregates. Analysis of the TEM image gave an average particle core size of 3.4 ± 1.8 nm (Figure 2.2c). These DLS and TEM results suggest the formation of a majority of individual Cat-MDBC/USNP colloids due to the occurrence of undesired aggregation being minimized through biphasic ligand exchange using Cat-MDBC.

The biphasic ligand exchange process with Cat-MDBC was further evaluated. First, inductively-coupled plasma mass spectrometry (ICP-MS) was used to determine Fe content in aqueous Cat-MDBC/USNP colloids (2.6 mL) (III in Figure 2.2a). Compared with Fe = 1.1 mg used in the recipe, the biphasic ligand exchange efficiency could be calculated to be $9.6 \pm 1.4\%$ (within 14% error with three freshly-prepared dispersions). This means that 9.6% USNPs in hexane phase was transferred to aqueous phase (see appendix A for detailed calculation). Next, thermogravimetric analysis (TGA) was used to determine the USNP contents in the formed Cat-MDBC/USNP colloids. As seen in Figure A5, the TGA trace of Cat-MDBC/USNPs shows two main weight losses: the initial loss at 0-200 °C corresponding to residual water and the other loss at 200-450 °C to stabilizing ligands (mainly Cat-MDBC). Considering $\approx 20\%$ residues at >450 °C for Cat-MDBC itself, the weight loss at 200-600 °C was used to calculate the content of Fe₃O₄ USNPs in Cat-MDBC/USNP colloids to be 9.6%, suggesting the actual mass ratio of Cat-MDBC/USNP = 9.4/1. This value implicates the presence of less USNPs in the colloids,

compared with 13.0 % of Fe₃O₄ USNPs estimated from the recipe based on the mass ratio of Cat-MDBC/OA-USNP = 5/1.

In another set, to examine the effect of the organic solvent on biphasic ligand exchange, the similar procedure was repeated with chloroform, instead of hexane as an organic solvent of OA-USNPs. As seen in Figure A6, the aqueous top layer was not clearly separated from the organic chloroform bottom layer after sonication. Further, the DLS diagram of the resultant Cat-MDBC/USNP colloids shows multimodal distribution. Such unsuccessful ligand exchange in chloroform/water system is plausibly due to the greater solubility of POEOMA blocks of Cat-MDBCs in chloroform than in water, compared with hexane. Hence, Cat-MDBC/USNPs with POEOMA coronas could be partitioned in both chloroform and water phases. However, in the hexane/water system, Cat-MDBC/USNPs with POEOMA coronas formed during ligand exchange could have lower tendency to be partitioned in hexane due to poor solubility of POEOMA coronas.

For comparison, COOH-MDBC (a precursor that was used for the EDC-mediated coupling reaction to synthesize Cat-MDBC) was examined for the biphasic ligand exchange method using the similar procedure with OA-USNP colloids dissolved in hexane. Different from Cat-MDBC (shown in Figure 2.2), the aqueous bottom layer was not clearly separated from the organic hexane layer after sonication. Furthermore, the DLS diagram of the resultant COOH-MDBC/USNP colloids shows multimodal distribution. These results suggest unsuccessful biphasic ligand exchange of COOH-MDBC on USNPs (Figure A7).

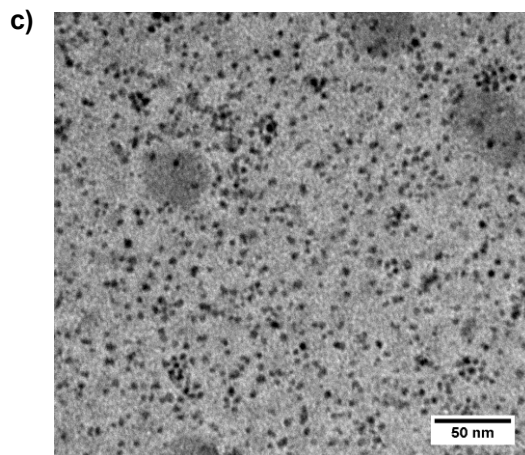
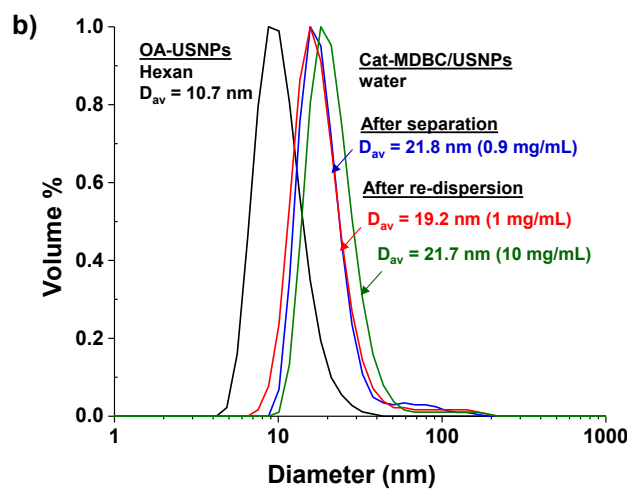
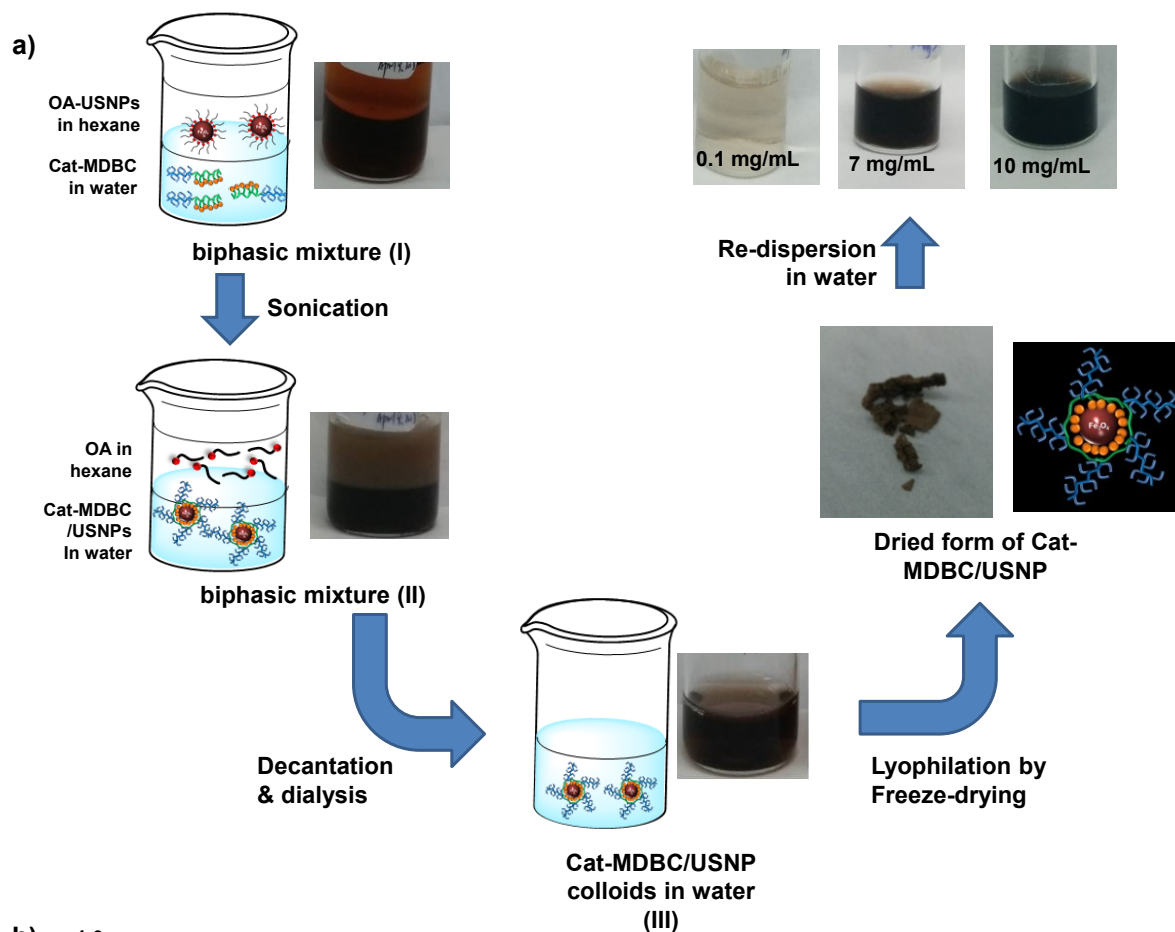


Figure 2.2. Schematic illustration of biphasic ligand exchange of OA-USNPs in hexane and cat-MDBC in water at the mass ratio of Cat-MDBC/USNP = 5/1 wt/wt (a), DLS diagrams (b), and TEM image (c) of aqueous Cat-MDBC/USNP colloids.

2.3.3 Non-cytotoxicity

To preliminarily assess aqueous Cat-MDBC/USNP colloids toward MRI applications, *in vitro* cytotoxicity with both HEC 293T normal and HeLa cancer cells were examined using MTT assay (a calorimetric method to measure cell toxicity). Aliquots of different concentrations of aqueous Cat-MDBC/USNP colloids were cultured with cells. Cells only were also included as controls. After 48 hr incubation, the absorbance was measured using absorbance-based plate reader and used to calculate cell viability. Figure 2.3 suggests >80% viability of both cells in the presence of aqueous Cat-MDBC/USNP colloids, suggesting non-cytotoxicity of aqueous Cat-MDBC/USNP colloids up to 200 $\mu\text{g/mL}$.

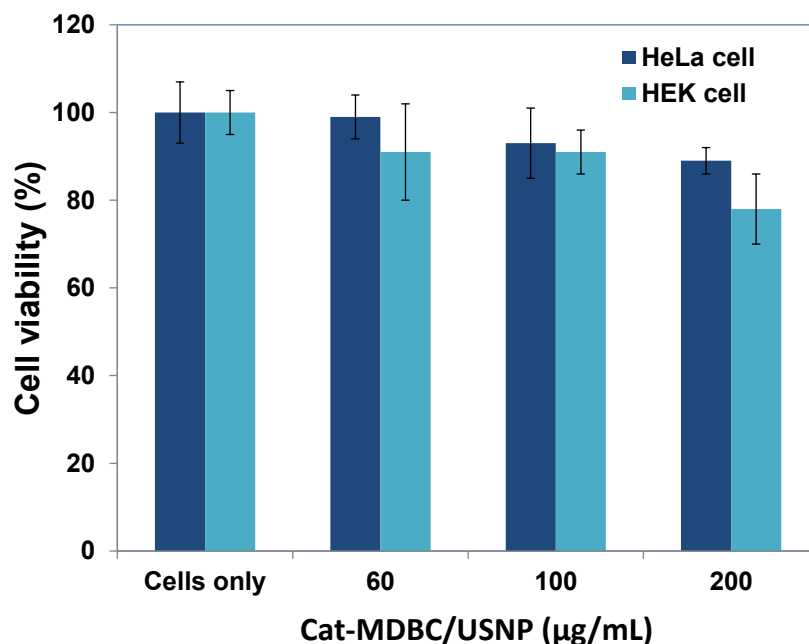


Figure 2.3. Viability of HEK 293T and HeLa cells cultured with various concentrations of aqueous Cat-MDBC/USNP colloids at 37 °C for 48 hrs, determined by MTT assay.

2.3.4 Excellent colloidal stability in various pH and physiological conditions

Excellent colloidal stability with no occurrence of large aggregation in biological conditions is critical to achieve prolonged blood retention time and optimal relaxometric properties for MRI since they are strongly affected by the size and surface charge of nanoparticles *in vivo*. Thus, zeta potential (ξ) of aqueous Cat-USNP/MDBC colloids was measured in 10 mM saline solution over pH. As seen in Figure 2.4a, the ξ of aqueous Cat-MDBC/USNP colloids is close to zero in a broad range of pH at 3-9, suggesting the surface of Cat-MDBC/USNP colloids presents to be neutral in physiological pH = 7.0-7.5. This result is greatly advantageous to endow prolonged colloidal stability in physiological conditions as well as minimize non-specific interactions with proteins in blood.¹⁰⁰ Additionally, the ξ of Cat-MDBC/USNP colloids is greater than that of Cat-MDBC itself which ranges at -15 - -30 mV at pH >7. Such difference of the ξ between Cat-MDBC/USNP colloids and Cat-MDBC could suggest that most catechol groups are bound to USNP surfaces in aqueous Cat-MDBC/USNP colloids.

To examine excellent colloidal stability, aliquots of aqueous Cat-MDBC/USNP colloids were incubated at different pHs. As seen in Figure 2.4b, their diameter kept unchanged in the broad range of pH = 4, 7, and 9 at 37 °C, suggesting no significant effect of pH on colloidal stability of neutral Cat-MDBC/USNP colloids. Next, aqueous Cat-MDBC/USNP colloids were then incubated with human serum in a physiological condition (pH = 7.3 at 37 °C). Figure 2.4c shows no occurrence of significant precipitation of Cat-MDBC/USNP colloids at both 0.4 and 1.7 mg/mL concentrations over 96 hrs. Further, aqueous Cat-MDBC/USNP colloids (1.2 mg) were incubated with human IgG protein (8 mg/mL) in a physiological condition (pH = 7.3 at 37 °C). IgG is found at 7-16 mg/mL in human blood stream. Even though the size and size distribution of Cat-MDBC/USNP colloids were similar to those of IgG proteins, DLS results

show no evidence of aggregation (Figure A8). Further to quantify the interaction of Cat-MDBC/USNPs with IgG, bicinchoninic acid (BCA) assay was used.¹⁰¹ As seen in Figure 2.4d, aqueous Cat-MDBC/USNP colloids exhibit no significant specific interactions with human IgG. These results suggest that Cat-MDBC/USNP colloids are colloiddally stable in the presence of proteins and do not exhibit significant protein absorption.

We now would like to provide the comparison of colloidal stability of Cat-MDBC/USNP colloids with COOH-MDBC/USNP colloids (Figure A9). Note that aqueous COOH-MDBC/USNP colloids with diameter ≈ 16 nm by DLS were prepared using conventional ligand exchange process (see appendix A), while aqueous Cat-MDBC/USNP colloids were prepared by biphasic ligand exchange. Similar to Cat-MDBC/USNP colloids, the formed COOH-MDBC/USNP colloids exhibit excellent colloidal stability in the presence of IgG protein (8 mg/mL) and in serum at pH = 7, although they had the $\xi \approx -10$ mV at the pH. They were also colloiddally-stable in a broad range of pH = 4-10. Given these promising results, animal studies should be conducted to better understand *in vivo* colloidal stability of both Cat-MDBC/USNP and COOH-MDBC/USNP colloids during blood circulation.

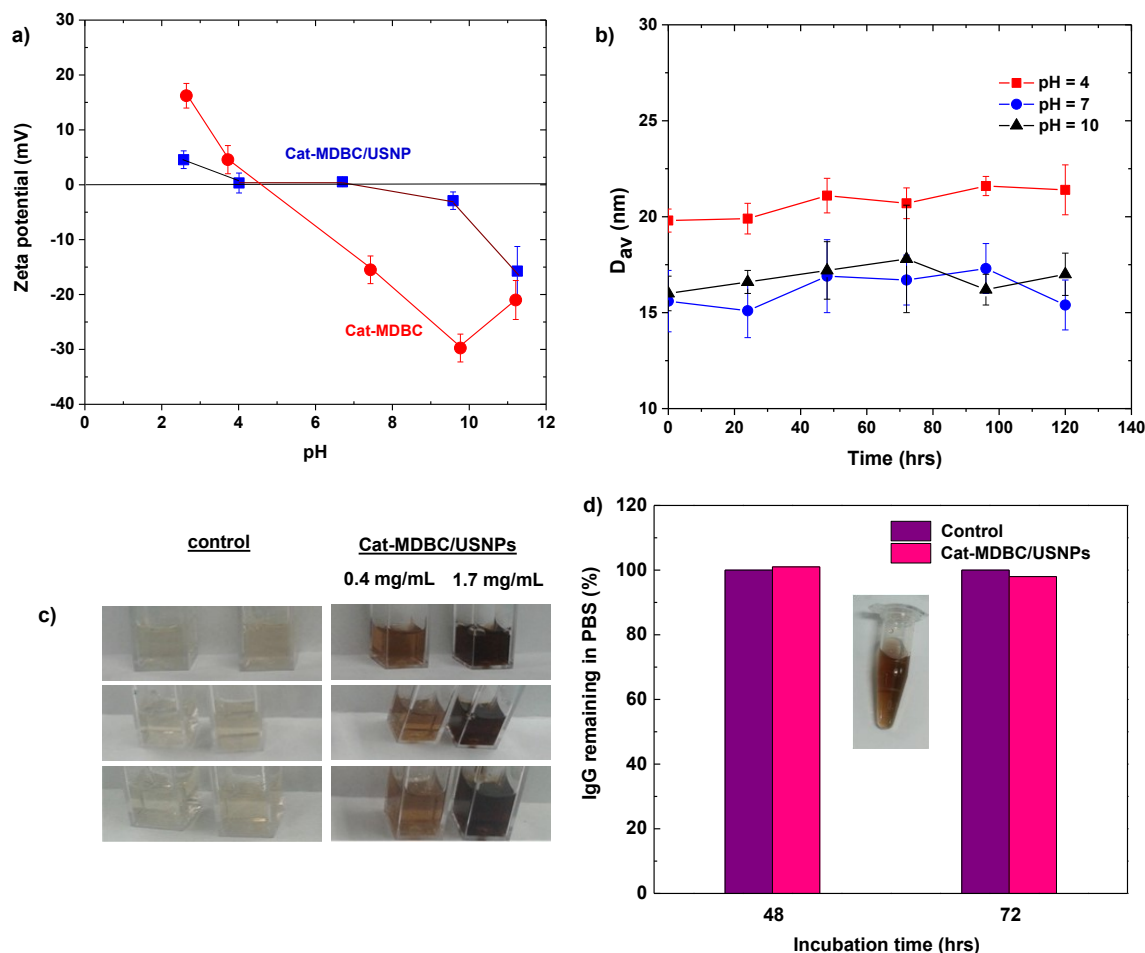


Figure 2.4. For aqueous Cat-MDBC/USNP colloids, evolution of their zeta potential over pH compared with Cat-MDBC (a), evolution of their diameter over time at various pH = 4, 7, and 10 (b), digital images of their mixtures with human serum at 0.4 and 1.7 mg/mL (c), and no significant interaction with IgG protein (8 mg/mL) over 72 hrs determined BCA assay (d). Inset in (d) shows the digital picture of their mixtures with IgG proteins after 72 hr incubation.

2.3.5 Relaxometric analysis and *in vitro* T_1 -weighted MRI.

To preliminarily evaluate aqueous Cat-MDBC/USNP colloids with excellent colloidal stability as an effective T_1 contrast agent, their relaxometric properties were determined at clinical magnetic field strengths (1.41 T, corresponding to 60 MHz). Longitudinal and transverse

magnetic relaxation times (T_1 and T_2 respectively) were measured on dilutions of the colloids (Figure 2.5). From the slopes, the relaxivity was determined to be $r_1 = 6.8 \text{ mM}^{-1}\text{s}^{-1}$ and $r_2/r_1 = 5.5$. These values are close to those expected for individual USNPs; for example, $r_1 = 10.7 \text{ mM}^{-1}\text{s}^{-1}$ and $r_2/r_1 = 3.6$ for commercially-available Supravist (SHU-555C)¹⁰² and $r_1 = 4.5\text{-}4.8 \text{ mM}^{-1}\text{s}^{-1}$ and $r_2/r_1 = 3.4 - 6.1$ for PEGylated USNPs.^{48, 64, 67} In addition, from the intercepts, $1/T_1 = 0.31 \text{ s}^{-1}$ and $1/T_2 = 0.88 \text{ s}^{-1}$ were estimated at $[\text{Fe}] = \text{zero}$ (meaning no presence of Cat-MDBC/USNP colloids; i.e. pure water). These values are similar to the reported $1/T_1 = 0.24 \pm 0.03 \text{ s}^{-1}$ and $1/T_2 = 0.8 \pm 0.1 \text{ s}^{-1}$ for pure water determined at 1.5 T.¹⁰³ This comparison validates the reliability of our determination of the relaxivity data. Further, *in vitro* T_1 -weighted MRI of aqueous Cat-MDBC/USNP colloids was conducted at clinical magnetic field strength (1.41 T). Their favorable relaxometric properties provide brighter T_1 -weighted imaging at as low as 0.38-0.57 mM Fe concentration. Promisingly, this concentration is significantly lower than that (0.9-1.9 mM Fe) for the corresponding COOH-MDBC having pendant carboxylates.⁵⁵ These results are promising in that Cat-MDBC/USNP colloids hold a great potential as an effective T_1 contrast agent with prolonged colloidal stability in physiological conditions.

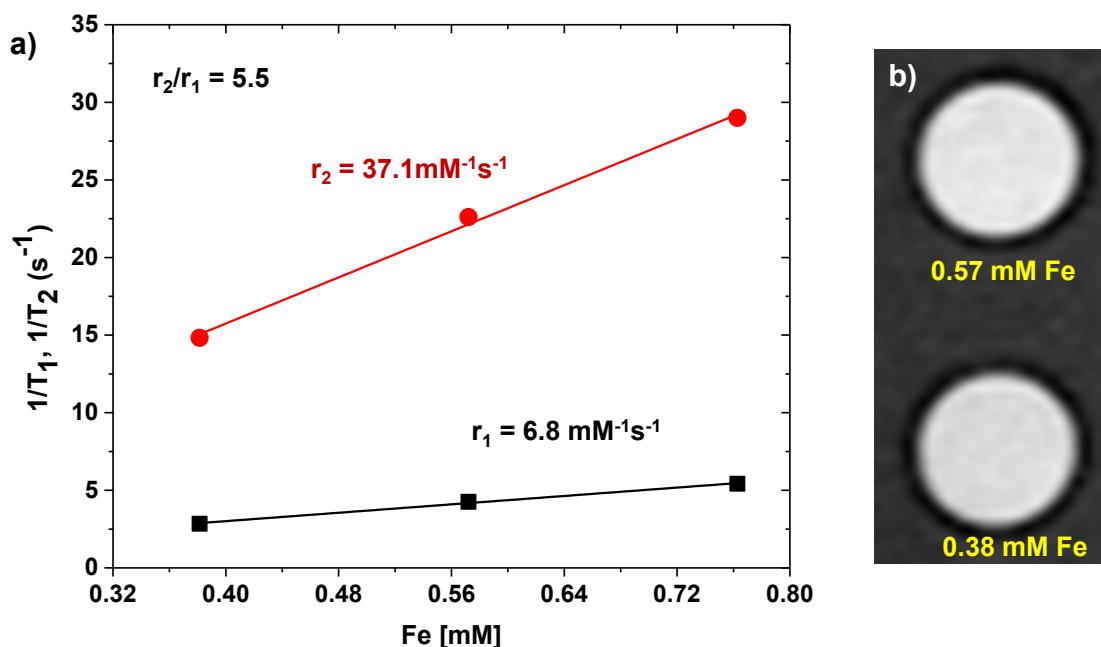


Figure 2.5. Relaxation rates ($1/T_1$ and $1/T_2$) and T_1 -weighted MRI for aqueous Cat-MDBC/USNP colloids at 1.41 T at 37 °C.

2.3.6 Multidentate: block vs. random copolymer (Cat-MDBC vs. Cat-MDRC)

The above results indicate that Cat-MDBC (block copolymer) enables the formation of aqueous single-layered Cat-MDBC/USNPs colloids with diameter ≈ 20 nm as an effective T_1 contrast enhancement agent for MRI. Here, we compare Cat-MDBC with the corresponding "multidentate random copolymer (Cat-MDRC)". Note that the density of pendant catechol groups in Cat-MDRC was designed to be similar to Cat-MDBC (Figure 2.6a).

Figure A10a illustrates our synthetic scheme of Cat-MDRC. First, COOH-MDRC was synthesized by two steps: 1) ATRP of OEOMA and tBMA to yield well-controlled random P(OEOMA-co-tBMA) with DP = 25 for OEOMA units and DP = 31 for tBMA units and 2) hydrolytic cleavage of pendant t-butoxy groups of tBMA units to the corresponding P(OEOMA-

co-MAA) (i.e. COOH-MDRC). Next, similar to Cat-MDBC, well-controlled Cat-MDRC was synthesized by the carbodiimide-mediated coupling reaction of pendant COOH groups of COOH-MDRC with amino groups of dopamine. ¹H-NMR of the resultant Cat-MDRC shows the presence of pendant catechol groups at 6.3-6.7 ppm (e), pendant OEO moieties at 4.0 ppm (b) and 3.2-3.7 ppm, backbone methyl groups at 0.7-1.1 ppm (c, d), and terminal phenyl groups at 7.3 ppm (a). Similar to Cat-MDBC, the integral ratio of the peaks (b, c, d, and e) was used to determine the extent of coupling reaction to be >90% (Figure A10b).

After the successful synthesis of Cat-MDRC, the similar procedure for biphasic ligand exchange was examined in aqueous solution at the mass ratio of Cat-MDRC/USNP = 5/1 wt/wt. Both DLS and TEM results suggest the formation of multimodal clusters of Cat-MDRC/USNP colloids with their average diameters to be 40 and 115 nm (Figure 2.6b and 2.6c). Further to see if the formation of large clusters is due to biphasic ligand exchange process, the conventional ligand exchange process was examined, where OA surface ligands were replaced with new Cat-MDRC ligands on USNPs in organic solution (chloroform/EtOH solvent mixture). The resulting Cat-MDBC/USNP colloids were dispersed in water, yielding clusters with the diameter to be 42.6 nm and large aggregates (diameter >1 μm) in aqueous solution (Figure A11 of DLS diagram). These results are different from the formation of single layered Cat-MDBC/USNP colloids; the plausible reason could be the random distribution of pendant catechol groups, compared to their spatial localization as a block.

Further, the cluster-like colloids presented transverse relaxivity constant $r_2 = 93.5 \text{ mM}^{-1}\text{s}^{-1}$, which is close to typical values of negative MRI contrast agents of clusters having SNPs with diameter $\approx 4 \text{ nm}^{104}$ (Figure 2.6d and 2.6e). This result suggests that Cat-MDRC forms aggregate-

like clusters with USNPs, which could be suitable for T_2 contrast enhancement, not for T_1 contrast enhancement.

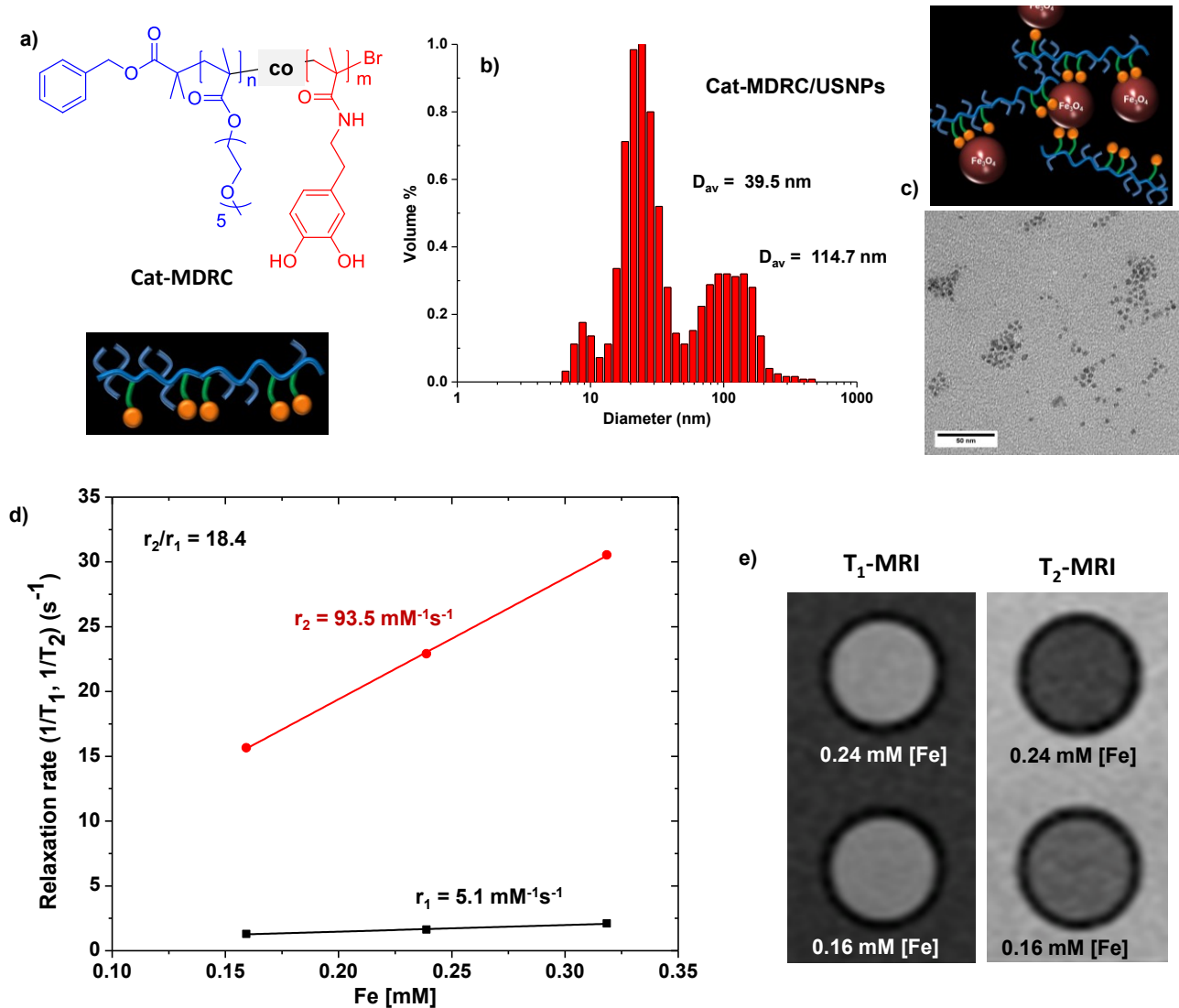


Figure 2.6. For Cat-MDRC, chemical structure (a), DLS diagram (b), TEM image (c), relaxation rates ($1/T_1$ and $1/T_2$) (d), and *in vitro* MRI at 1.41 T at 37 °C (e).

2.4 Conclusion

Well-controlled Cat-MDBC having pendant catechol groups in the anchoring block strongly bound to USNP surfaces was synthesized by consecutive ATRP followed by post-modification methods. The Cat-MDBC was proved to be an effective multidentate that enabled the replacement of originally-stabilizing monodentates (oleic acids) on USNP surfaces, allowing for the fabrication of aqueous Cat-MDBC/USNP colloids with diameter <20 nm through the biphasic ligand exchange process. The resulting colloids are non-toxic to cells up to 200 $\mu\text{g/mL}$. They exhibit excellent colloidal stability in a broad range of pH = 4-10 as well as in the presence of IgG model protein and even in human serum, plausibly due to the nature of pendant catechol groups being neutral in charges, combined with the presence of pendant oligo(ethylene glycol)-containing polymethacrylate providing excellent hydrophilic sheaths. Different from Cat-MDBC, Cat-MDRC (the counterpart of Cat-MDBC) formed undesired clusters of USNP colloids as aggregates, not single layered Cat-MDRC/USNP colloids, by both biphasic and conventional ligand exchange. These results, combined with the relaxivity and *in vitro* MRI results, suggest that aqueous Cat-MDBC/USNP colloids hold a great potential as an effective contrast agents for vascular MRI diagnosis.

Chapter 3: Extremely small-sized Fe₃O₄ nanoparticles as MRI contrast agents

3.1 Introduction

In chapter 2, I demonstrate that mussel-inspired multidentate block copolymer strategy is an effective and versatile method to stabilize USNPs with the diameter ≈ 3 nm. The aqueous Cat-MDBC/USNP colloids fabricated by biphasic ligand exchange process exhibit excellent colloidal stability in physiological conditions, in the presence of protein, and in human serum. They have higher r_1 value ($6.8 \text{ mM}^{-1}\text{s}^{-1}$) and relatively lower r_2/r_1 value (5.5), suggesting effective T_1 -contrast agents. To be comparable with Gd³⁺-based T_1 -contrast agents with $r_2/r_1 < 2$, the magnetic properties of Fe₃O₄ nanoparticles should be further improved. A recent report describes that extremely small Fe₃O₄ nanoparticles (ESNPs) with diameter < 3 nm can be applicable because they have smaller magnetic moment and can improve the image quality of T_1 -weighted MRI.^{9, 105} Inspired by these reports of ESPNP colloids, this chapter describes our preliminary results from my efforts to exploit our mussel-inspired Cat-MDBC strategies towards ESNPs with diameter < 2 nm as effective bright T_1 -contrast agents. After the surface functionalization with Cat-MDBC, the Cat-MDBC/ESNPs were further characterized and compared with Cat-MDBC/USNPs with 3.5 nm core.

3.2 Experimental

The detailed experimental procedures and conditions including material, instruments and analysis of NMR, TGA, biphasic ligand exchange, colloidal stability in the presence of IgG, cell viability, relaxivity and *in vitro* MRI are described in the previous chapter.

3.2.1 Synthesis of oleic acid stabilized ESNPs (OA-ESNPs)

The OA-stabilized ESNPs were synthesized follow the procedures described in publication.^{105, 106} For the synthesis of iron-oleate complex precursor, FeCl₃ (0.65 g 4 mmol) was mixed with sodium oleate (3.65 g, 12 mmol) in 4/3/7 v/v/v EtOH/H₂O/hexane mixture (28 mL). The mixture was heated at 70°C for 4 hrs and cooled to room temperature. The upper organic layer was separated and washed with water (10 mL) three times. Solvents were removed by a rotary evaporation and residues were dried in a vacuum oven at room temperature for 24 hrs. In the next step, the synthesized iron-oleate complex (1.8 g) was mixed with oleyl alcohol (3.22 g, 12 mmol) in diphenyl ether (10g). After being degased at 90 °C under vacuum for 2 hrs, the mixture was heated to 200 °C at 10 °C/min and kept at the same temperature for 30 mins under N₂ atmosphere. The whole system was rapidly cooled to room temperature and then precipitated from acetone. The products were dried in a vacuum oven at room temperature for 24 hrs, yielding OA-ESNPs brown, sticky solids.

3.2.2 Synthesis of Cat-MDBC

Well-controlled Cat-MDBC was synthesized by a combination of ATRP and post-modification methods as described in chapter 2. The precursor POEOMA-b-PtBMA synthesized by ATRP had the DP of 25 for POEOMA block and 27 for PtBMA block by ¹H-NMR.

3.2.3 UV-Vis spectroscopic titration

UV-Vis titrations were performed using a UV/Vis/NIR spectrometer (B&W Tek i-Trometer) equipped with BDS130 UV/Vis/NIR light source. All titrations were conducted under magnetic stirring in quartz cuvette at room temperature. First, blanked the UV machine using 2.5 mL pH 7 Tris-HCl buffer. Prepared aqueous Cat-MDBC (MW = 13500 g/mol) in Tris-HCl buffer of pH = 7 at 2.6 mg/mL concentration. An aliquot of the polymer solution (0.2 mL, 0.038 μ mol Cat-MDBC) was mixed with Tris-HCl buffer (2.5 mL). Measured the UV-visible absorption of the resulting mixture before titration. Titration of this stock solution was conducted using FeCl₃ aqueous solution at 1.3 mg/mL under magnetic stirring. Each time 25 μ L FeCl₃ (0.2 μ mol) aqueous solution was added to Cat-MDBC stock solution and was stirred for 2 mins before UV-visible absorption measurement. UV-Vis titration experiments were performed in duplicate for Cat-MDBC. Similarly, UV-Vis titration of dopamine hydrochloride using FeCl₃ was performed. Prepared dopamine hydrochloride (MW = 189.6 g/mol) in Tris-HCl buffer of pH = 7 at 0.95 mg/mL concentration. An aliquot of the dopamine hydrochloride solution (0.2 mL, 1 μ mol dopamine hydrochloride) was mixed with Tris-HCl buffer (2.5 mL). Measured the UV-visible absorption of the resulting mixture before titration. Titration of this stock solution was conducted using 1.3 mg/mL FeCl₃ water solution following same process as Cat-MDBC titration. Following the similar process, 0.2 mL 2.97 mg/mL Cat-MDBC/ESNPs in Tris-HCl buffer of pH = 7 (containing Cat-MDBC 0.038 μ mol) was mixed with Tris-HCl buffer (2.5 mL) and titrated using 1.3 mg/mL FeCl₃ aqueous solution.

3.2.4 Colloidal stability in physiological conditions

For colloidal stability in physiological conditions, Cat-MDBC/ESNPs were directly dispersed in PBS at 0.5 mg/mL. The colloidal was incubated at 37 °C over five days.

3.3 Results and Discussion

Well-defined OA-ESNPs was synthesized using heat-up method as reported in literature.¹⁰⁵ The resulting OA-ESNPs have their diameter = 5.7 ± 0.2 nm dispersed in hexane by DLS (Figure 3.1b) and the core diameter = 2.1 ± 0.4 nm by TEM. Note that the particle morphologies are not clearly defined (Figure 3.1a).

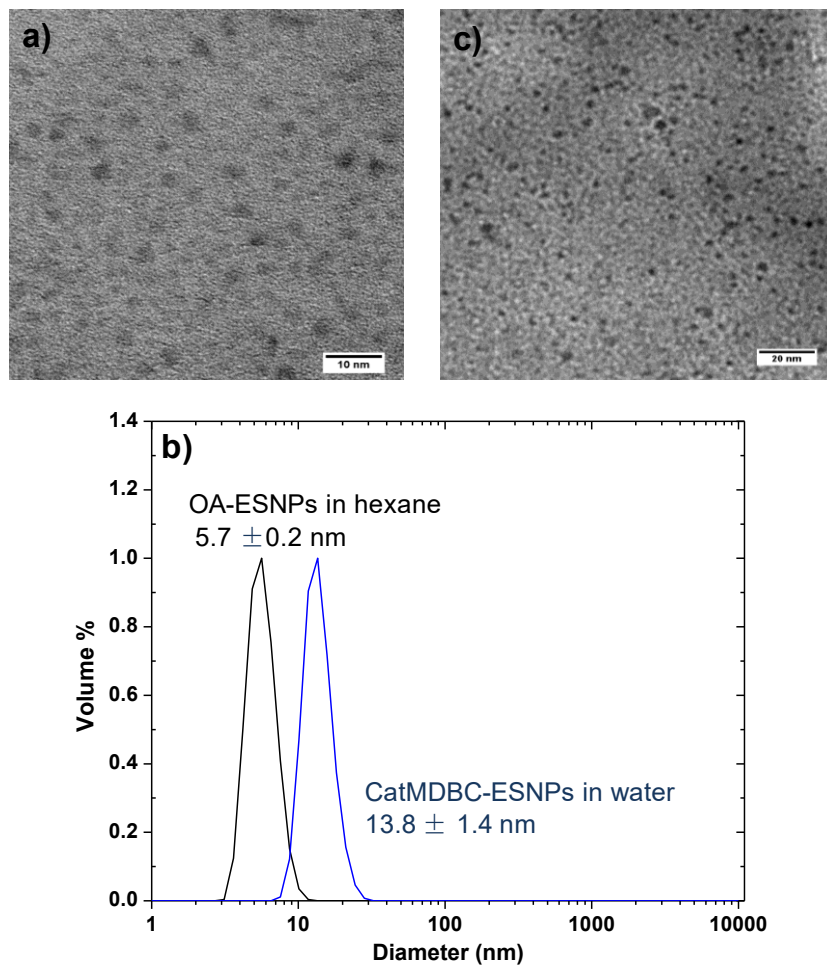


Figure 3.1. TEM image of OA-ESNPs (a), and Cat-MDBC/ESNP colloids (c). DLS diagrams of OA-ESNPs in hexane at 0.5 mg/mL and Cat-MDBC/ESNPs in water at 0.5 mg/mL (b).

For the fabrication of ESNPs stabilized with Cat-MDBC in aqueous solution (aqueous Cat-MDBC/ESNP colloids), our biphasic ligand exchange process was examined. As reported, a biphasic mixture of aqueous solution of Cat-MDBC and organic solution of OA-ESNPs in hexane was subjected to sonication at room temperature. The aqueous layer carefully taken was subjected to intensive dialysis over distilled water and then lyophilized using freeze-drier. The

dried Cat-MDBC/ESNPs colloids were readily re-dispersed in aqueous solution at various concentrations. The Cat-MDBC/ESNPs have hydrodynamic diameter to be ≈ 13.8 nm by DLS (Figure 3.1b) and TEM results indicate the core diameter of ESNPs in individual Cat-MDBC/ESNPs colloids to be 1.9 ± 0.6 nm (Figure 3.1c). The dried Cat-MDBC/ESNPs were analyzed through thermogravimetric analysis (TGA) to determine the content of ESNPs in the dried colloids (Figure B1 in appendix B). The ESNPs content in Cat-MDBC/ESNPs was calculated to be 14.1%.

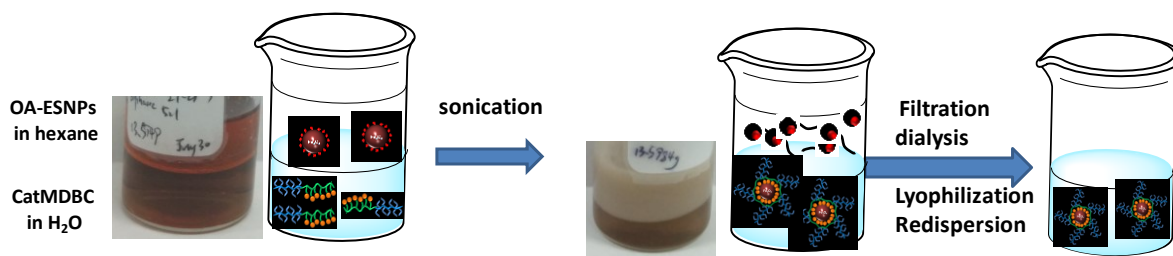


Figure 3.2. Biphasic ligand exchange of OA-ESNPs in hexane and cat-MDBC in water at the mass ratio of Cat-MDBC/ESNP = 5/1 wt/wt.

Further, we have attempted to determine the percentage of free catechol groups not bound to ESNPs surface using UV-Vis spectroscopic titration. This method follows UV-Vis absorbance at 570 nm as a result of the formation of complex between catechol groups and Fe^{3+} ions in aqueous solution in pH 7.^{107, 108} First, UV-Vis titration of dopamine hydrochloride in pH = 7 Tris-HCl buffer reveals the equivalent of Fe^{3+} : catechol = 1:1, which indicates the 1:1 ratio of Fe^{3+} : catechol in complex (appendix B, Figure B2). The molar absorptivities of Fe^{3+} -catechol complex at different wavelength were also obtained (appendix B, Figure B3). The UV-Vis titration spectral changes of Cat-MDBC using Fe^{3+} at same condition are quite similar to that of dopamine hydrochloride. With the continuous addition of Fe^{3+} (0.2 μmol each time) and the

formation of complex ($\lambda_{\text{max}} = 570 \text{ nm}$), the UV-Vis spectra first show increasing absorbance at 570 nm then reach the plateau corresponding to the saturation of all the catechol groups in the polymer by Fe^{3+} . Since Cat-MDBC exhibits no absorbance at 570 nm, the increasing absorbance at 570 nm from beginning point to the plateau (0.28 ± 0.01) is proportion to the concentration of Fe(III)-catechol complex as well as the initial concentration of catechol groups. We further conducted UV-Vis titration of Cat-MDBC/ESNPs having same amount of Cat-MDBC (using the Cat-MDBC% information from TGA), the absorbance at 570 nm before addition of Fe^{3+} iron corresponds to the binding of catechol with the surface of ESNPs. The increasing absorbance at 570 nm from beginning point to the plateau (0.14 ± 0.01) is proportion to the concentration of Fe(III)-catechol complex formed by Fe^{3+} irons in titrating solution and catechol groups which were not bound to the surface of ESNPs. Through calculation (refer to appendix B for details), the unbound catechol percentage in Cat-MDBC/ESNPs is determined to be 50%.

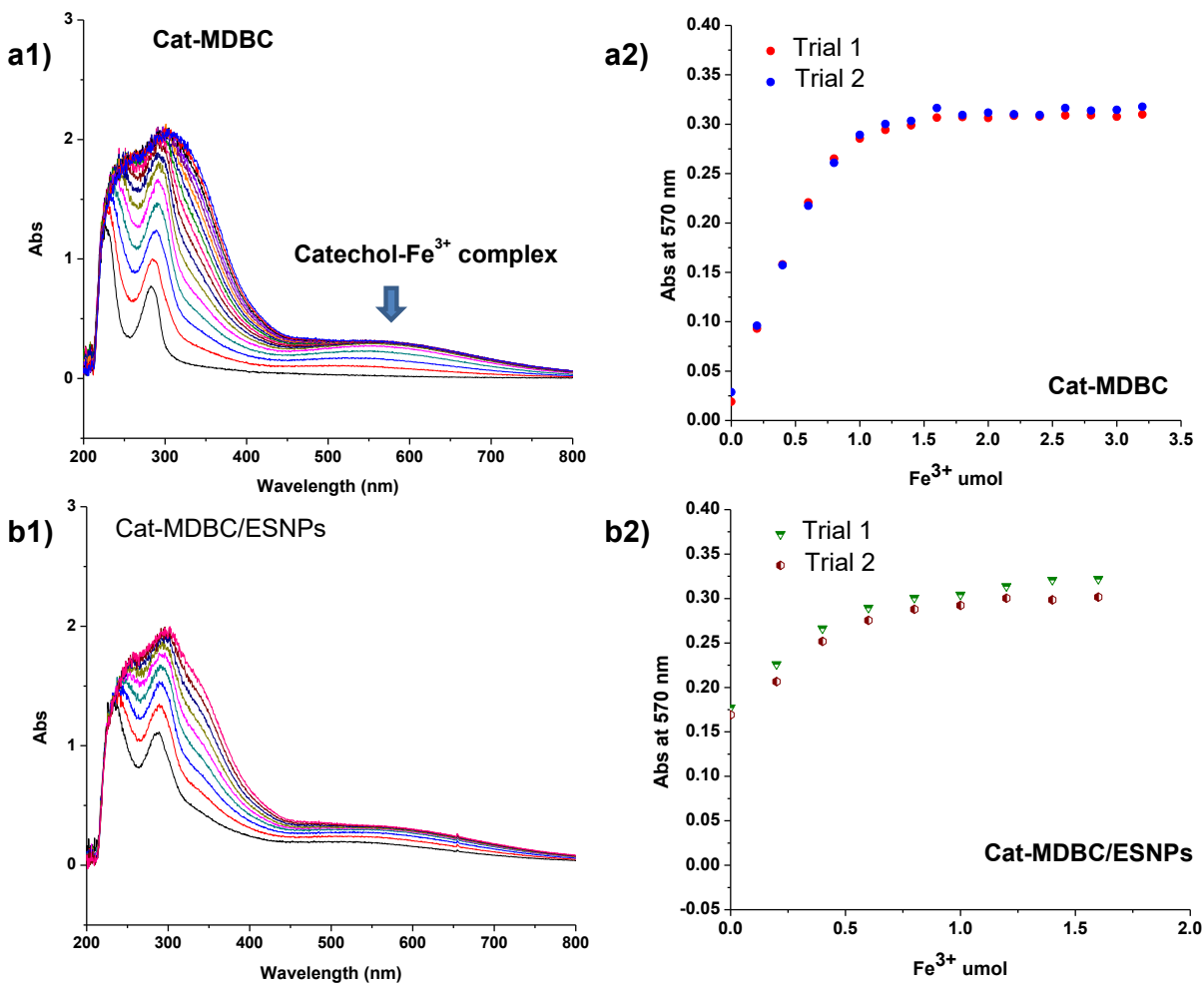


Figure 3.3. UV–Vis spectroscopic monitoring during titration of Cat-MDBC (a1), Cat-MDBC/ESNPs (b1). Profiles of the absorbance at 570 nm with the addition of the Fe^{3+} into Cat-MDBC (a2), Cat-MDBC/ESNPs (b2).

Next, the formed Cat-MDBC/ESNP colloids were preliminarily assessed toward MRI applications. Firstly, *in vitro* cytotoxicity with both HEC 293T normal and HeLa cancer cells were examined using MTT assay. As seen in Figure 3.4, the viability of both cells was >80% in the presence of aqueous Cat-MDBC/ESNP colloids, suggesting non-cytotoxicity of aqueous Cat-MDBC/USNP colloids up to 200 $\mu\text{g}/\text{mL}$, similar to Cat-MDBC/USNP colloids

Secondly, colloidal stabilities of the Cat-MDBC/ESNPs were examined in physiological condition (in PBS buffer at pH = 7.4) and in the presence of IgG protein at 37 °C. As seen in Figure 3.4a, the diameter of Cat-MDBC/ESNP colloids remained stable in PBS solution at 37 °C. Then, aqueous Cat-MDBC/ESNP colloids (1.2 mg) were incubated with human IgG protein (8 mg/mL) in a physiological condition (pH = 7.3 at 37 °C). Their size and size distribution kept unchanged by DLS (Figure 3.4b) and no occurrence of significant interactions with human IgG was observed by BCA assay (Figure 3.4d). These results suggest that Cat-MDBC/ESNP colloids are colloiddally stable in the presence of proteins and prevents from protein adsorption in physiological conditions.

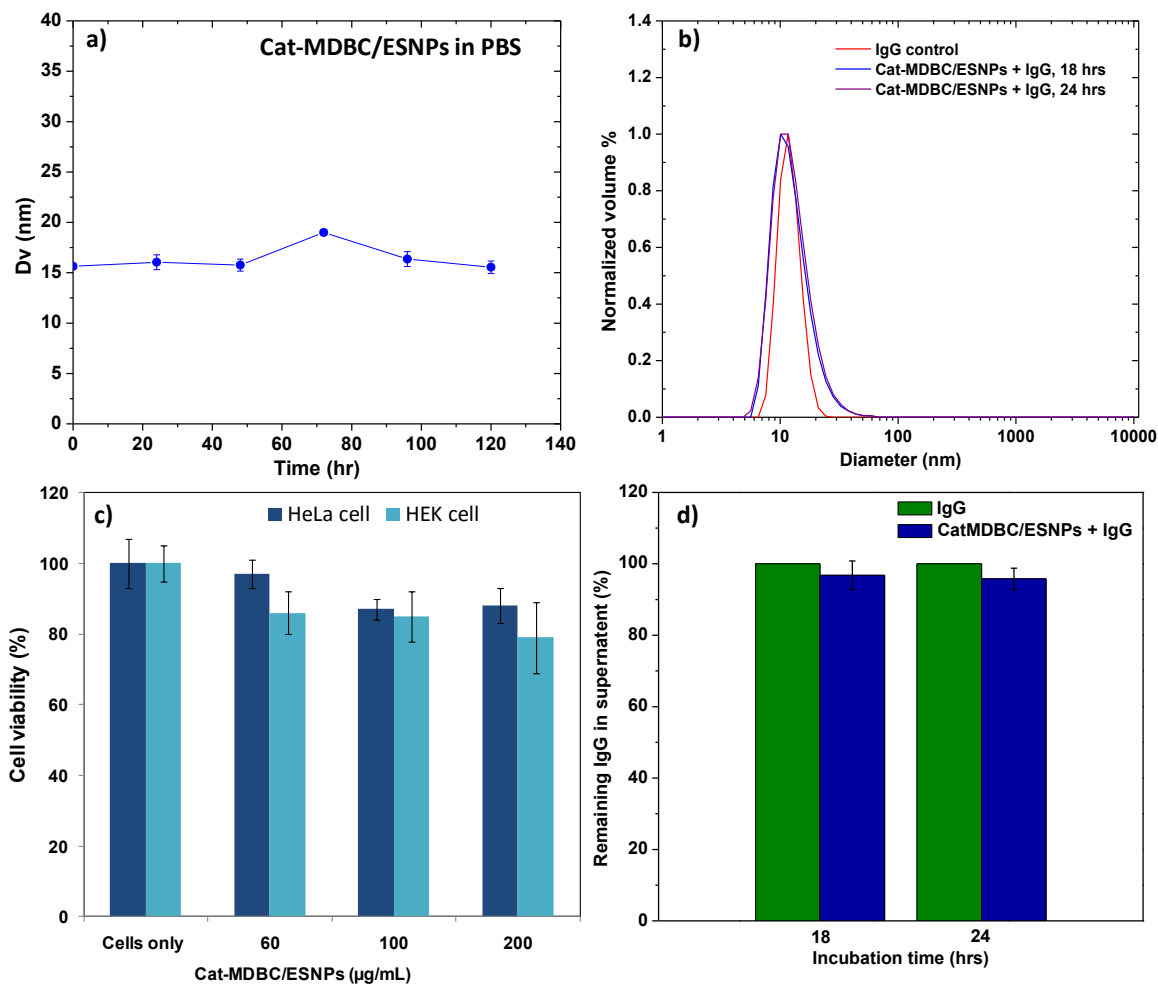


Figure 3.4. For aqueous Cat-MDBC/ESNP colloids evolution of their diameter over time in PBS at 37 °C (a), and DLS traces of Cat-MDBC/ESNPs and IgG incubated for 18 hrs and 24 hrs at 37 °C (b), Viability of HEK 293T and HeLa cells cultured with various concentrations of aqueous Cat-MDBC/ESNP colloids at 37 °C for 48 hrs, determined by MTT assay (c) and interaction of Cat-MDBC/ESNPs with IgG proteins over 24 hrs determined BCA assay (d).

Thirdly, the colloiddally-stable aqueous Cat-MDBC/ESNPs as an effective T_1 contrast agent were characterized with their relaxometric properties at clinical magnetic field strengths (1.41 T,

corresponding to 60 MHz). Longitudinal and transverse magnetic relaxation times measurements (T_1 and T_2 respectively) were performed on dilutions of the colloids (Figure 3.5). From the slopes, the relaxivity parameters were determined to be $r_1 = 3.0 \text{ mM}^{-1}\text{s}^{-1}$ and $r_2/r_1 = 1.5$. As compared in relaxivity parameters in Table 3.1, the r_2/r_1 value of Cat-MDBC/ESNPs is significantly lower than Cat-MDBC/USNPs and Supravist with their core diameter $>3 \text{ nm}$ and promisingly are comparable with that $r_2/r_1 = 1.4$ of Gd^{3+} -based T_1 -contrast agents (PEG- Gd_2O_3). T_1 signal enhancement (bright image) was observed at low concentration of Fe of $0.22 \sim 0.32 \text{ mM}$. These results, together with the r_1 and r_2 values mentioned above, suggest that Cat-MDBC/ESNPs can be promising candidate as T_1 -weighted MRI contrast agents and competitive alternative for Gadolinium-based contrast agents.

Table 3.1. Size and relaxivity parameters (r_2 , r_2/r_1) of various contrast agents measured at 1.4 T

	Core	D_{TEM} (nm)	r_2 ($\text{mM}^{-1}\text{s}^{-1}$)	r_2/r_1	ref
Cat-MDBC/ESNPs	Fe_3O_4	2	4.6	1.5	This work ¹⁰⁹
Cat-MDBC/USNPs	Fe_3O_4	3.5	37.1	5.5	
Supravist (SHU-555C)	Fe_3O_4	3-5	38.5	3.6	¹¹⁰
PEG- Gd_2O_3	Gd_2O_3	3	13.4	1.4	¹¹¹

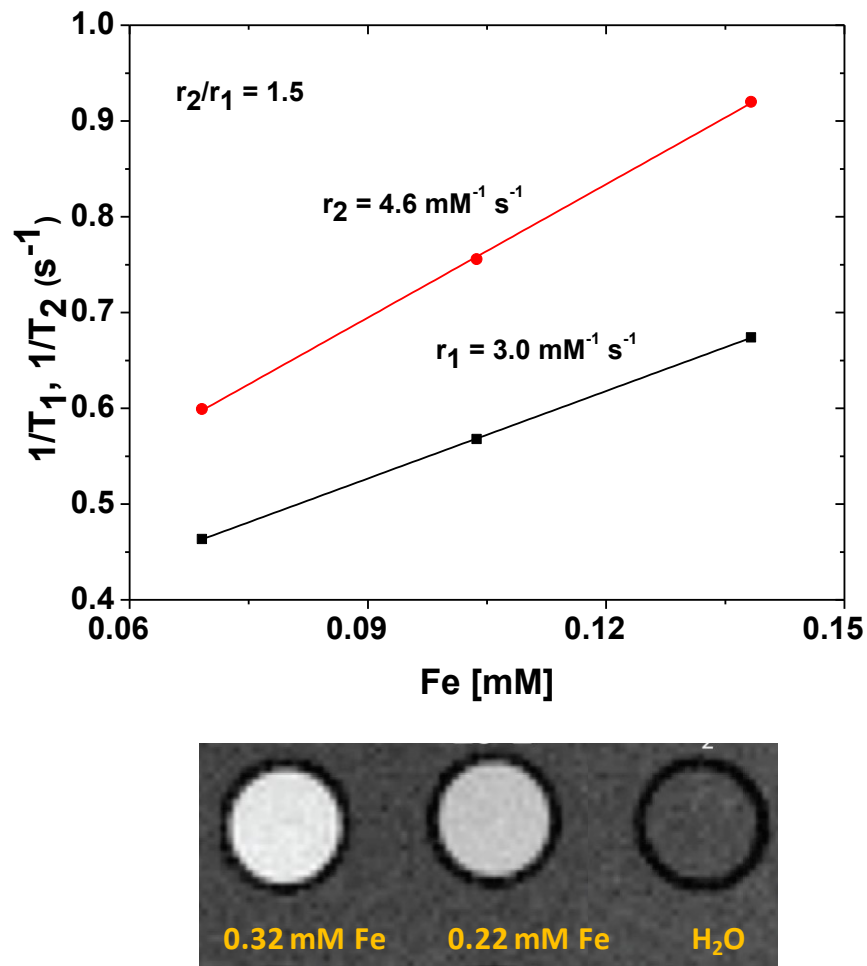


Figure 3.5. Relaxation rates ($1/T_1$ and $1/T_2$) and T_1 -weighted MRI for aqueous Cat-MDBC/ESNP colloids at 1.41 T at 37 °C.

3.4 Conclusion

ESNPs with core diameter <2 nm were successfully synthesized and coated with Cat-MDBC. The resulting Cat-MDBC/ESNPs colloids with diameter <17 nm exhibit excellent colloidal stability in physiological conditions (PBS, 37 °C) and in the presence of IgG, owing to hydrophilic sheath from POEOMA block. The *in vitro* MRI and relaxivity results suggest that decrease in size of iron oxide nanoparticle dramatically decreases the T_2 effect of Cat-

MDBC/ESNPs, thus providing great potential of Cat-MDBC/ESNPs as a promising biocompatible alternative to Gd^{3+} -based T_1 -weighted MRI contrast agents.

Chapter 4: Conclusion and Future work

A combination of ATRP and post-modification methods were utilized to synthesize well-controlled catechol functionalized block copolymers (Cat-MDBC) having pendant catechol groups in anchoring block and pendant oligo (ethylene glycol) in the hydrophilic block. They were revealed to be effective multidentate ligands to stabilize USNPs with core diameter = 3.5 nm and ESNPs with core diameter = 2 nm in physiological conditions. The new Cat-MDBC/USNPs and ESNPs colloids were proved to be valuable as T_1 -MRI contrast agents. The influence of ligand exchange method (biphasic vs. homogenous), architectures of stabilizers (random copolymer Cat-MDRC vs. block copolymer Cat-MDBC) and different types of anchoring groups (carboxylate vs. catechol) on the properties of copolymer-USNPs complex were explored in detail in Chapter 2. The Cat-MDBC/USNPs colloids (hydrodynamic diameter <20 nm) obtained by biphasic ligand exchange exhibit excellent colloidal stability as well as promising relaxivity properties and effective T_1 -MRI signal enhancement. The influences of the core size of iron oxide nanoparticle on relaxivity properties are discussed in chapter 3. After decreasing the size of SNPs from 3.5 nm (USNPs) to 2 nm (ESNPs), the Cat-MDBC/ESNPs fabricated by biphasic ligand exchange exhibit less T_2 effect and comparable relaxivity property with Gd^{3+} -based T_1 -contrast agents. The current design of the Cat-MDBC and the biphasic ligand exchange process can be improved in the future. For example, the density of unbound catechol groups in Cat-MDBC/ESNP colloids might be reduced by optimizing the catechol groups in Cat-MDBC. Further, a considerable effort should be made to improve the efficiency of biphasic ligand exchange. In addition, the *in vivo* experiments should be conducted to further evaluate the properties of Cat-MDBC/USNPs and Cat-MDBC/ESNPs as the MRI contrast agents, such as their distribution in organs, metabolic process and blood circulation time.

References

1. P. Lauterbur, *Nature* 1973, 242, 190-191.
2. S. Huettel, A. Song and G. McCarthy, *Functional Magnetic Resonance Imaging*. Sinauer Associates, 2004.
3. C. F. Geraldès and S. Laurent, *Contrast media & molecular imaging*, 2009, 4, 1-23.
4. S. Xue, H. Yang, J. Qiao, F. Pu, J. Jiang, K. Hubbard, K. Hekmatyar, J. Langley, M. Salarian, R. C. Long, R. G. Bryant, X. P. Hu, H. E. Grossniklaus, Z.-R. Liu and J. J. Yang, *Proceedings of the National Academy of Sciences*, 2015, 112, 6607-6612.
5. P. Caravan, J. J. Ellison, T. J. McMurry and R. B. Lauffer, *Chemical Reviews*, 1999, 99, 2293-2352.
6. M. A. Sieber, T. Steger-Hartmann, P. Lengsfeld and H. Pietsch, *Journal of Magnetic Resonance Imaging*, 2009, 30, 1268-1276.
7. R. Agarwal, S. M. Brunelli, K. Williams, M. D. Mitchell, H. I. Feldman and C. A. Umscheid, *Nephrology Dialysis Transplantation*, 2009, 24, 856-863.
8. T. Grobner, *Nephrology Dialysis Transplantation*, 2006, 21, 1104-1108.
9. N. Lee and T. Hyeon, *Chemical Society Reviews*, 2012, 41, 2575-2589.
10. A. E. Merbach and E. Toth, *The Chemistry of Contrast Agents in Medical Magnetic Resonance Imaging*, Wiley, 2001.
11. Y. Anzai, C. W. Piccoli, E. K. Outwater, W. Stanford, D. A. Bluemke, P. Nurenberg, S. Saini, K. R. Maravilla, D. E. Feldman, U. P. Schmiedl, J. A. Brunberg, I. R. Francis, S. E. Harms, P. M. Som and C. M. Tempany, *Radiology*, 2003, 228, 777-788.
12. S. G. Ruehm, C. Corot, P. Vogt, S. Kolb and J. F. Debatin, *Circulation*, 2001, 103, 415-422.

13. A. Elias and A. Tsourkas, *ASH Education Program Book*, 2009, 2009, 720-726.
14. W. Stöber, A. Fink and E. Bohn, *Journal of Colloid and Interface Science*, 1968, 26, 62-69.
15. T. Tago, T. Hatsuta, K. Miyajima, M. Kishida, S. Tashiro and K. Wakabayashi, *Journal of the American Ceramic Society*, 2002, 85, 2188-2194.
16. Y. Lu, Y. Yin, B. T. Mayers and Y. Xia, *Nano letters*, 2002, 2, 183-186.
17. D. K. Yi, S. S. Lee, G. C. Papaefthymiou and J. Y. Ying, *Chemistry of Materials*, 2006, 18, 614-619.
18. J.-I. Park and J. Cheon, *Journal of the American Chemical Society*, 2001, 123, 5743-5746.
19. E. E. Carpenter, C. Sangregorio and C. J. O'Connor, *Magnetics, IEEE Transactions on*, 1999, 35, 3496-3498.
20. Z. Ban, Y. A. Barnakov, F. Li, V. O. Golub and C. J. O'Connor, *Journal of Materials Chemistry*, 2005, 15, 4660.
21. E. E. Carpenter, *Journal of Magnetism and Magnetic Materials*, 2001, 225, 17-20.
22. J. Lin, W. Zhou, A. Kumbhar, J. Wiemann, J. Fang, E. E. Carpenter and C. J. O'Connor, *Journal of Solid State Chemistry*, 2001, 159, 26-31.
23. S. Sun and H. Zeng, *Journal of the American Chemical Society*, 2002, 124, 8204-8205.
24. A. K. Gupta and M. Gupta, *Biomaterials*, 2005, 26, 3995-4021.
25. Y. Sahoo, A. Goodarzi, M. T. Swihart, T. Y. Ohulchanskyy, N. Kaur, E. P. Furlani and P. N. Prasad, *The Journal of Physical Chemistry B*, 2005, 109, 3879-3885.
26. S. Wagner, J. Schnorr, H. Pilgrim, B. Hamm and M. Taupitz, *Investigative Radiology*, 2002, 37, 167-177.

27. N. Fauconnier, A. Bee, J. Roger and J. N. Pons, *Trends in Colloid and Interface Science X*, eds. C. Solans, M. R. Infante and M. J. García-Celma, Steinkopff, 1996, vol. 100, pp. 212-216.
28. N. Fauconnier, J. N. Pons, J. Roger and A. Bee, *Journal of Colloid and Interface Science*, 1997, 194, 427-433.
29. E. Dubois, R. Perzynski, F. Boué and V. Cabuil, *Langmuir*, 2000, 16, 5617-5625.
30. Y. Sahoo, H. Pizem, T. Fried, D. Golodnitsky, L. Burstein, C. N. Sukenik and G. Markovich, *Langmuir*, 2001, 17, 7907-7911.
31. D. I. Kreller, G. Gibson, W. Novak, G. W. Van Loon and J. H. Horton, *Colloids and Surfaces A: Physicochemical and Engineering Aspects*, 2003, 212, 249-264.
32. D. I. Kreller, G. Gibson, G. W. vanLoon and J. H. Horton, *Journal of Colloid and Interface Science*, 2002, 254, 205-213.
33. A. K. Yuen, G. A. Hutton, A. F. Masters and T. Maschmeyer, *Dalton Transactions*, 2012, 41, 2545-2559.
34. H. Basti, L. B. Tahar, L. Smiri, F. Herbst, M.-J. Vaulay, F. Chau, S. Ammar and S. Benderbous, *Journal of Colloid and Interface Science*, 2010, 341, 248-254.
35. H. Gu, Z. Yang, J. Gao, C. Chang and B. Xu, *Journal of the American Chemical Society*, 2005, 127, 34-35.
36. B. P. Lee, P. B. Messersmith, J. N. Israelachvili and J. H. Waite, *Annual Review of Materials Research*, 2011, 41, 99.
37. C. C. Berry, S. Wells, S. Charles and A. S. G. Curtis, *Biomaterials*, 2003, 24, 4551-4557.
38. R. S. Molday and D. Mackenzie, *Journal of Immunological Methods*, 1982, 52, 353-367.
39. Y. X. Wang, *Quantitative Imaging in Medicine and Surgery*, 2011, 1, 35-40.

40. K. G. Paul, T. B. Frigo, J. Y. Groman and E. V. Groman, *Bioconjugate Chemistry*, 2004, 15, 394-401.
41. M. Carmen Bautista, O. Bomati-Miguel, M. del Puerto Morales, C. J. Serna and S. Veintemillas-Verdaguer, *Journal of Magnetism and Magnetic Materials*, 2005, 293, 20-27.
42. D. Liu, W. Wu, J. Ling, S. Wen, N. Gu and X. Zhang, *Advanced Functional Materials*, 2011, 21, 1498-1504.
43. E. L. Bentzen, I. D. Tomlinson, J. Mason, P. Gresch, M. R. Warnement, D. Wright, E. Sanders-Bush, R. Blakely and S. J. Rosenthal, *Bioconjugate Chemistry*, 2005, 16, 1488-1494.
44. S. Tong, S. Hou, Z. Zheng, J. Zhou and G. Bao, *Nano Letters*, 2010, 10, 4607-4613.
45. J.-C. Boyer, M.-P. Manseau, J. I. Murray and F. C. J. M. van Veggel, *Langmuir*, 2010, 26, 1157-1164.
46. M. Kamimura, D. Miyamoto, Y. Saito, K. Soga and Y. Nagasaki, *Langmuir*, 2008, 24, 8864-8870.
47. M. Chastellain, A. Petri and H. Hofmann, *Journal of Colloid and Interface Science*, 2004, 278, 353-360.
48. N. Chan, M. Laprise-Pelletier, P. Chevallier, A. Bianchi, M.-A. Fortin and J. K. Oh, *Biomacromolecules*, 2014, 15, 2146-2156.
49. J. M. Harris and R. B. Chess, *Nature Reviews Drug Discovery*, 2003, 2, 214-221.
50. R. B. Liebherr, T. Soukka, O. S. Wolfbeis and H. H. Gorris, *Nanotechnology*, 2012, 23, 485103.
51. Y. Nagasaki, T. Kutsuna, M. Iijima, M. Kato, K. Kataoka, S. Kitano and Y. Kadoma, *Bioconjugate Chemistry*, 1995, 6, 231-233.

52. C. Albornoz and S. E. Jacobo, *Journal of Magnetism and Magnetic Materials*, 2006, 305, 12-15.
53. D. J. Siegwart, J. K. Oh and K. Matyjaszewski, *Progress in Polymer Science*, 2012, 37, 18-37.
54. J.-F. Lutz, *Journal of Polymer Science Part A: Polymer Chemistry*, 2008, 46, 3459-3470.
55. N. Chan, P. Li and J. K. Oh, *ChemPlusChem*, 2014, 79, 1342-1351.
56. N. Lee and T. Hyeon, *Chemical Society Reviews.*, 2012, 41, 2575-2589.
57. C. Sun, J. S. H. Lee and M. Zhang, *Advanced Drug Delivery Reviews*, 2008, 60, 1252-1265.
58. W. Chen, D. P. Cormode, Z. A. Fayad and W. J. M. Mulder, *Nanomedicine and Nanobiotechnology*, 2011, 3, 146-161.
59. M. E. Lobatto, V. Fuster, Z. A. Fayad and M. J. M. Mulder, *Nature Reviews Drug Discovery*, 2011, 10, 835-852.
60. F. Hu and Y. S. Zhao, *Nanoscale*, 2012, 4, 6235-6243.
61. H. B. Na, I. C. Song and T. Hyeon, *Advanced Materials*, 2009, 21, 2133-2148.
62. H. Duan, M. Kuang, X. Wang, Y. A. Wang, H. Mao and S. Nie, *Journal of Physical Chemistry C*, 2008, 112, 8127-8131.
63. F. Hu, Q. Jia, Y. Li and M. Gao, *Nanotechnology*, 2011, 22, 245604/245601-245604/245607.
64. B. H. Kim, N. Lee, H. Kim, K. An, Y. I. Park, Y. Choi, K. Shin, Y. Lee, S. G. Kwon, H. B. Na, J.-G. Park, T.-Y. Ahn, Y.-W. Kim, W. K. Moon, S. H. Choi and T. Hyeon, *Journal of the American Chemical Society*, 2011, 133, 12624-12631.

65. L. Sandiford, A. Phinikaridou, A. Protti, L. K. Meszaros, X. Cui, Y. Yan, G. Frodsham, P. A. Williamson, N. Gaddum, R. M. Botnar, P. J. Blower, M. A. Green and R. T. M. de Rosales, *ACS Nano*, 2013, 7, 500-512.
66. U. I. Tromsdorf, O. T. Bruns, S. C. Salmen, U. Beisiegel and H. Weller, *Nano Letters.*, 2009, 9, 4434-4440.
67. J. Y. Park, P. Daksha, G. H. Lee, S. Woo and Y. Chang, *Nanotechnology*, 2008, 19, 365603/365601-365603/365607.
68. E. Amstad, M. Textor and E. Reimhult, *Nanoscale*, 2011, 3, 2819-2843.
69. D. Ling, N. Lee and T. Hyeon, *Accounts of Chemical Research*, 2015, 48, 1276-1285.
70. H.-J. Chung, H.-S. Lee, K. H. Bae, Y.-H. Lee, J.-N. Park, S.-W. Cho, J.-Y. Hwang, H.-W. Park, R. Langer, D. Anderson and T.-G. Park, *ACS Nano*, 2011, 5, 4329-4336.
71. T. Zhang, J. Ge, Y. Hu and Y. Yin, *Nano Letters.*, 2007, 7, 3203-3207.
72. J. K. Oh and J. M. Park, *Progress in Polymer Science.*, 2011, 36, 168-189.
73. J.-F. Lutz, S. Stiller, A. Hoth, L. Kaufner, U. Pison and R. Cartier, *Biomacromolecules*, 2006, 7, 3132-3138.
74. X. Lu, R. Jiang, M. Yang, Q. Fan, W. Hu, L. Zhang, Z. Yang, W. Deng, Q. Shen, Y. Huang, X. Liu and W. Huang, *Journal of Materials Chemistry B: Materials for Biology and Medicine*, 2014, 2, 376-386.
75. J. S. Basuki, A. Jacquemin, L. Esser, Y. Li, C. Boyer and T. P. Davis, *Polymer Chemistry*, 2014, 5, 2611-2620.
76. Y. Zhong, F. Dai, H. Deng, M. Du, X. Zhang, Q. Liu and X. Zhang, *Journal of Materials Chemistry B: Materials for Biology and Medicine*, 2014, 2, 2938-2946.
77. M. Kumagai, M. R. Kano, Y. Morishita, M. Ota, Y. Imai, N. Nishiyama, M. Sekino, S. Ueno, K. Miyazono and K. Kataoka, *Journal of Controlled Release*, 2009, 140, 306-311.

78. V. Torrisi, A. Graillet, L. Vitorazi, Q. Crouzet, G. Marletta, C. Loubat and J. F. Berret, *Biomacromolecules*, 2014, 15, 3171-3179.
79. S. Moulay, *Polymer Reviews*, 2014, 54, 436-513.
80. A. K. L. Yuen, G. A. Hutton, A. F. Masters and T. Maschmeyer, *Dalton Transactions*, 2012, 41, 2545-2559.
81. L.-S. Xiao, J.-T. Li, D. F. Brougham, E. K. Fox, N. Feliu, A. Bushmelev, A. Schmidt, N. Mertens, F. Kiessling, M. Valldor, B. Fadeel and S. Mathur, *ACS Nano*, 2011, 5, 6315-6324.
82. E. Amstad, T. Gillich, I. Bilecka, M. Textor and E. Reimhult, *Nano Letters.*, 2009, 9, 4042-4048.
83. C. Xu, K. Xu, H. Gu, R. Zheng, H. Liu, X. Zhang, Z. Guo and B. Xu, *Journal of the American Chemical Society*, 2004, 126, 9938-9939.
84. T. Gillich, C. Acikgoez, L. Isa, A. D. Schluter, N. D. Spencer and M. Textor, *ACS Nano*, 2013, 7, 316-329.
85. R. C. Stone, B. Qi, D. Trebatoski, R. Jetti, Y. P. Bandera, S. H. Foulger and O. T. Mefford, *Journal of Materials Chemistry B: Materials for Biology and Medicine*, 2014, 2, 4789-4793.
86. E. Amstad, A. U. Gehring, H. Fischer, V. V. Nagaiyanallur, G. Hahner, M. Textor and E. Reimhult, *Journal of Physical Chemistry C*, 2011, 115, 683-691.
87. M. Martin, P. Salazar, R. Villalonga, S. Campuzano, J. M. Pingarron and J. L. Gonzalez-Mora, *Journal of Materials Chemistry B: Materials for Biology and Medicine*, 2014, 2, 739-746.
88. H. B. Na, G. Palui, J. T. Rosenberg, X. Ji, S. C. Grant and H. Mattoussi, *ACS Nano*, 2012, 6, 389-399.

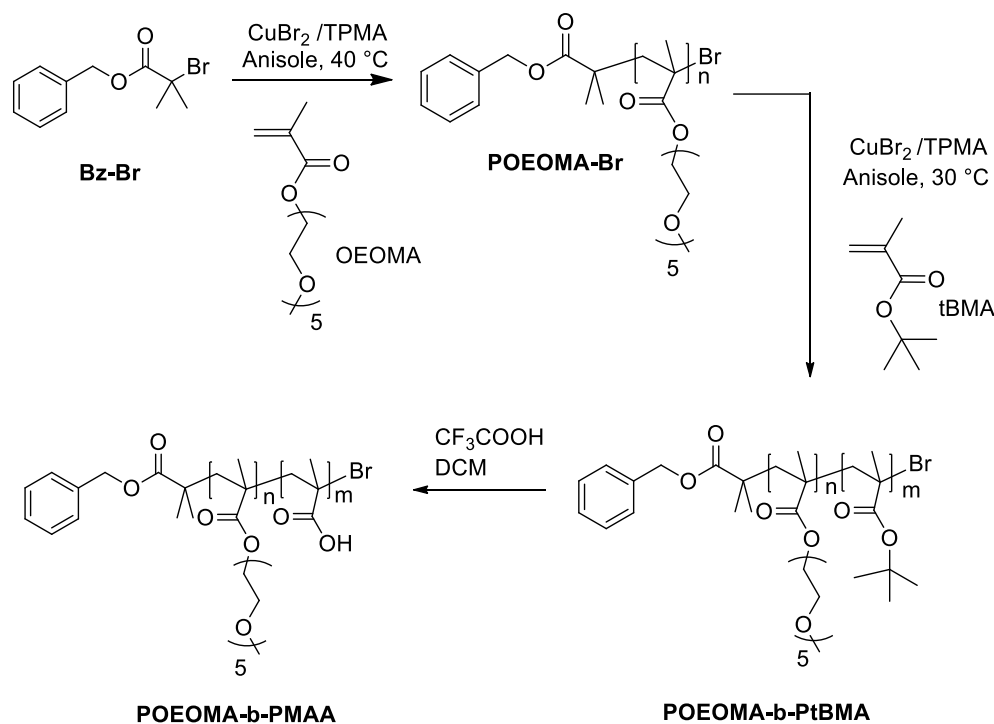
89. M. I. Shukoor, F. Natalio, H. A. Therese, M. N. Tahir, V. Ksenofontov, M. Panthoefer, M. Eberhardt, P. Theato, H. C. Schroeder, W. E. G. Mueller and W. Tremel, *Chemistry of Materials*, 2008, 20, 3567-3573.
90. Y. Lee, H. Lee, Y. B. Kim, J. Kim, T. Hyeon, H. Park, P. B. Messersmith and T. G. Park, *Advanced Materials*, 2008, 20, 4154-4157.
91. D. Ling, W. Park, Y. I. Park, N. Lee, F. Li, C. Song, S.-G. Yang, S. H. Choi, K. Na and T. Hyeon, *Angewandte Chemie International Edition*, 2011, 50, 11360-11365.
92. L. Brannon-Peppas, *Journal of Controlled Release*, 2000, 66, 321.
93. K. Knop, R. Hoogenboom, D. Fischer and U. S. Schubert, *Angewandte Chemie International Edition*, 2010, 49, 6288-6308.
94. J. Xie, C. Xu, N. Kohler, Y. Hou and S. Sun, *Advanced Materials*, 2007, 19, 3163-3166.
95. G. J. P. Britovsek, J. England and A. J. P. White, *Inorganic Chemistry*, 2005, 44, 8125-8134.
96. S. Y. An, J. W. Hwang, K. N. Kim, H. W. Jung, S. M. Noh and J. K. Oh, *Journal of Polymer Science, Part A: Polymer Chemistry*, 2014, 52, 572-581.
97. M. Kamigaito, T. Ando and M. Sawamoto, *Chemical Reviews*, 2001, 101, 3689-3745.
98. K. Matyjaszewski and J. Xia, *Chemical Reviews*, 2001, 101, 2921-2990.
99. E. D. Smolensky, H.-Y. E. Park, T. S. Berquo and V. C. Pierre, *Contrast Media & Molecular Imaging*, 2011, 6, 189-199.
100. S. Patil, A. Sandberg, E. Heckert, W. Self and S. Seal, *Biomaterials*, 2007, 28, 4600-4607.
101. Y. Wen and J. K. Oh, *Colloids and Surfaces, B: Biointerfaces*, 2015, 133, 246-253.
102. G. H. Simon, J. von Vopelius-Feldt, Y. Fu, J. Schlegel, G. Pinotek, F. Wendland Michael, M.-H. Chen and E. Daldrup-Link Heike, *Investigative Radiology*, 2006, 41, 45-51.

103. M. Rohrer, H. Bauer, J. Mintorovitch, M. Requardt and H.-J. Weinmann, *Investigative Radiology*, 2005, 40, 715-724.
104. H. Ai, C. Flask, B. Weinberg, X. Shuai, M. D. Pagel, D. Farrell, J. Duerk and J. Gao, *Advanced Materials*, 2005, 17, 1949-1952.
105. B. H. Kim, N. Lee, H. Kim, K. An, Y. I. Park, Y. Choi, K. Shin, Y. Lee, S. G. Kwon, H. B. Na, J. G. Park, T. Y. Ahn, Y. W. Kim, W. K. Moon, S. H. Choi and T. Hyeon, *Journal of the American Chemical Society*, 2011, 133, 12624-12631.
106. J. Park, K. An, Y. Hwang, J. G. Park, H. J. Noh, J. Y. Kim, J. H. Park, N. M. Hwang and T. Hyeon, *Nature Materials*, 2004, 3, 891-895.
107. T. B. Karpishin, M. S. Gebhard, E. I. Solomon and K. N. Raymond, *Journal of the American Chemical Society*, 1991, 113, 2977-2984.
108. P. Sánchez, N. Gálvez, E. Colacio, E. Miñones and J. M. Domínguez-Vera, *Dalton Transactions*, 2005, 811-813.
109. P. Li, P. Chevallier, P. Ramrup, D. Biswas, D. Vuckovic, M.-A. Fortin and J. K. Oh, *Chemistry of Materials*, 2015.
110. G. H. Simon, J. von Vopelius-Feldt, Y. Fu, J. Schlegel, G. Pinotek, M. F. Wendland, M.-H. Chen and H. E. Daldrup-Link, *Investigative Radiology*, 2006, 41, 45-51.
111. M.-A. Fortin, R. M. Petoral Jr, F. Söderlind, A. Klasson, M. Engström, T. Veres, P.-O. Käll and K. Uvdal, *Nanotechnology*, 2007, 18, 395501.

Appendix A

I) Synthesis and characterization of COOH-MDBC

Figure A1. Synthetic route to COOH-MDBC by consecutive ATRP and hydrolytic cleavage.



Synthesis of POEOMA-Br macroinitiators. Bz-Br (0.19 g, 0.75 mmol), OEOMA (16.9 g, 0.06 mol), CuBr_2 (11.2 mg, 50 μmol), TPMA (43.6 mg, 0.15 mmol), and anisole (16.1 g) were mixed in a 50 mL Schlenk flask. The mixture was deoxygenated by purging under nitrogen for 1 hr and then placed in an oil bath at $30\text{ }^\circ\text{C}$. A nitrogen pre-purged solution of $\text{Sn}(\text{EH})_2$ (28.5 mg, 70.3 μmol) dissolved in anisole (0.75 g) was injected into the Schlenk flask to initiate polymerization. Polymerization was stopped after 1 hr by cooling the reaction mixture in an ice bath and exposing it to air.

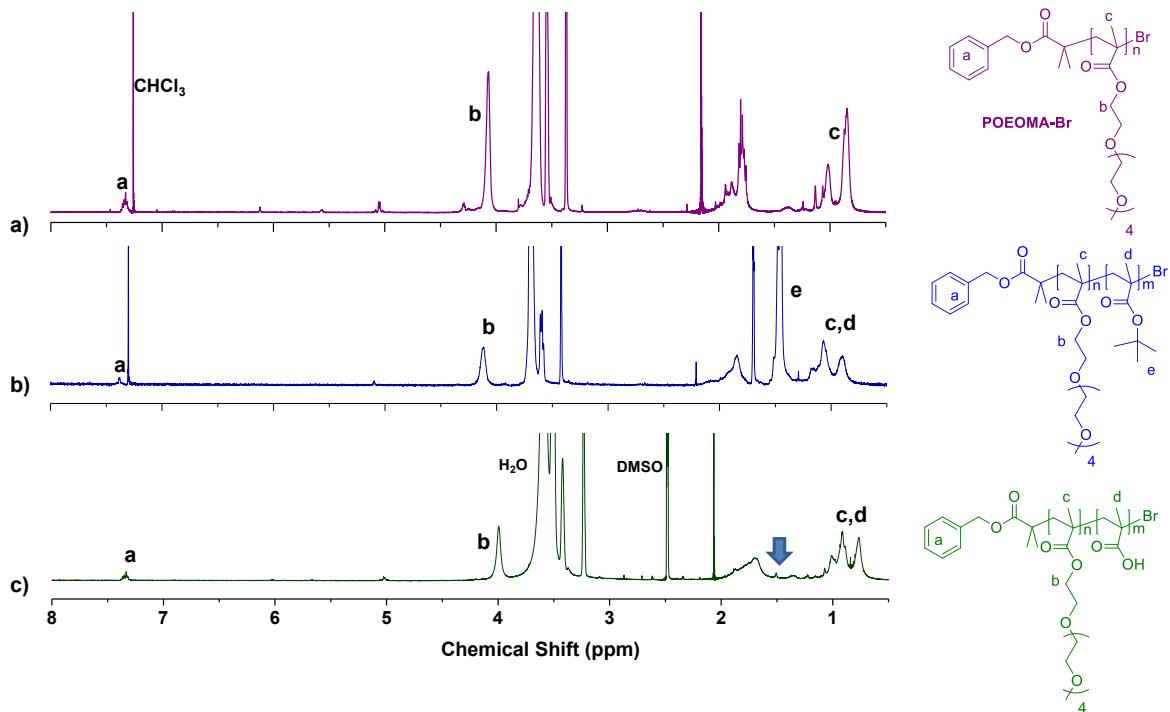
For purification, the as-synthesized polymer solution was precipitated from cold hexane three times to remove unreacted monomers. The precipitates were dissolved in acetone and then

passed through a column filled with basic alumina three times to remove residual copper species. The polymer solution was passed through a 0.2 μm PTFE filter to remove residual tin species. Solvents were removed by rotary evaporation and the residues were dried in a vacuum oven at room temperature for 24 hrs, yielding well-controlled POEOMA-Br macroinitiators (MI) having $M_n = 7,800$ g/mol and $M_w/M_n = 1.24$.

Synthesis of POEOMA-b-PtBMA. POEOMA-Br (1.3 g, 0.16 mmol), tBMA (1.8 g, 12.8 mmol), CuBr_2 (1.8 mg, 8.0 μmol), TPMA (7 mg, 24 μmol), and anisole (6.75 g) were mixed in a 25 mL Schlenk flask. The mixture was deoxygenated by purging under nitrogen for 1 hr, and then placed in an oil bath at 40 $^\circ\text{C}$. A nitrogen pre-purged solution of $\text{Sn}(\text{EH})_2$ (25.8 mg, 63.8 μmol) dissolved in anisole (0.5 g) was injected into the Schlenk tube to initiate polymerization. Polymerization was stopped after 3 hr by cooling the reaction mixture in an ice bath and exposing it to air. Similar procedure to purify the resulting block copolymers was used as described above to yield POEOMA-b-PtBMA having $M_n = 9,300$ g/mol and $M_w/M_n = 1.24$.

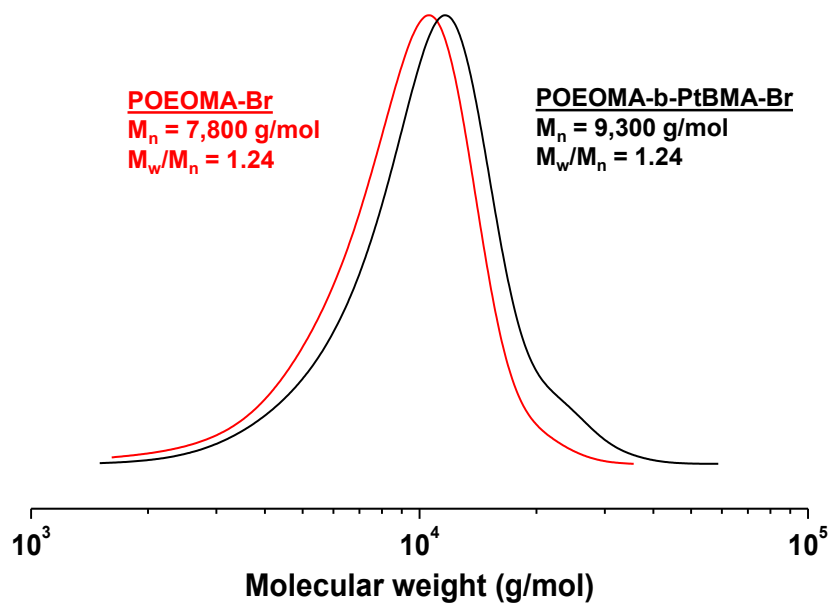
Hydrolytic cleavage to synthesize POEOMA-b-PMAA (COOH-MDBC). The purified, dried POEOMA-b-PtBMA (0.4 g, 56.5 μmol) dissolved in dichloromethane (DCM, 8 mL) was mixed with 10 fold excess of TFA under stirring for 24 hrs. The resulting mixtures were concentrated using rotary evaporation and precipitated from cold hexane three times. The precipitates were then dried in a vacuum oven at room temperature for 24 hrs. After cleavage, the previous PtBMA block turned to PMAA (poly(methacrylic acid)) block.

Figure A2. $^1\text{H-NMR}$ spectra of POEOMA-Br (a), POEOMA-*b*-PtBMA (b) in CDCl_3 , and POEOMA-*b*-PMAA in DMSO-d_6 (c).



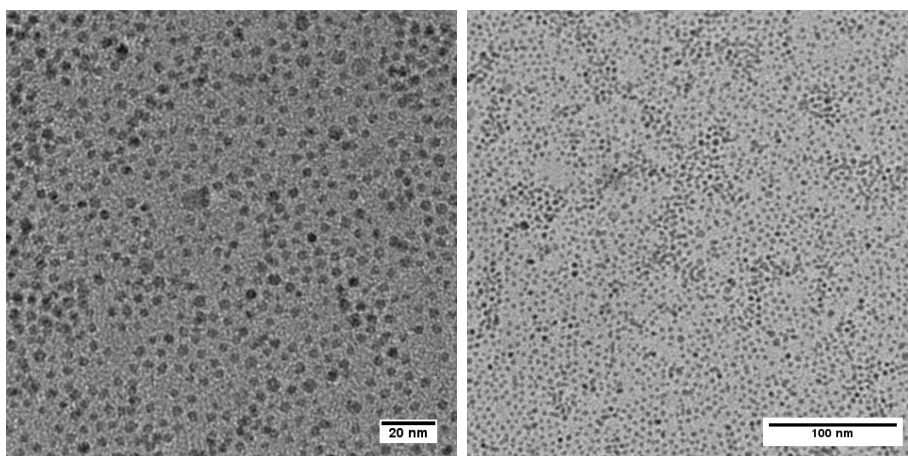
The degree of polymerization (DP) was determined from the integral ratio of peaks $[(c/3)/(a/5)]$ for POEOMA-Br to be 25 and peaks $[(e/9)/(b/2)]$ for POEOMA-*b*-PtBMA to be 25.

Figure A3. GPC traces of POEOMA-Br and POEOMA-b-PtBMA.



II) Biphasic ligand exchange

Figure A4. TEM images with different magnifications of OA-USNPs.



Calculation of biphasic ligand exchange efficiency by ICP measurements:

From ICP measurements, Fe = 37.8 ppm in 2.6 mL recovered water phase after biphasic ligand exchange. Thus, Fe = 0.098 mg. From the recipe, OA-USNPs = 2 mg; Fe₃O₄ content in OA-Fe₃O₄ = 75% by TGA and Fe content in Fe₃O₄ = 72.4% by elemental calculation. Thus, Fe = 2 mg × 0.75 × 0.724 = 1.09 mg (assuming that all Fe₃O₄ NPs in hexane are transferred to aqueous phase during biphasic ligand exchange process) Thus, efficiency = 0.098 mg/1.09 mg × 100 = 9%.

Figure A5. TGA trace of Cat-MDBC/USNP, compared with those of OA-USNPs and Cat-MDBC.

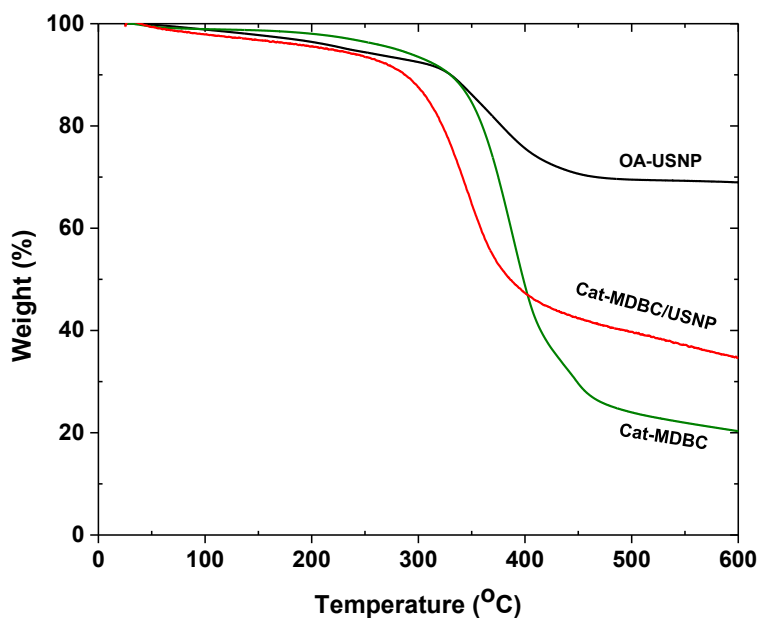


Figure A6. DLS diagram and digital image (inset) of Cat-MDBC/USNP colloids in water, prepared by biphasic ligand exchange process with chloroform as an organic phase.

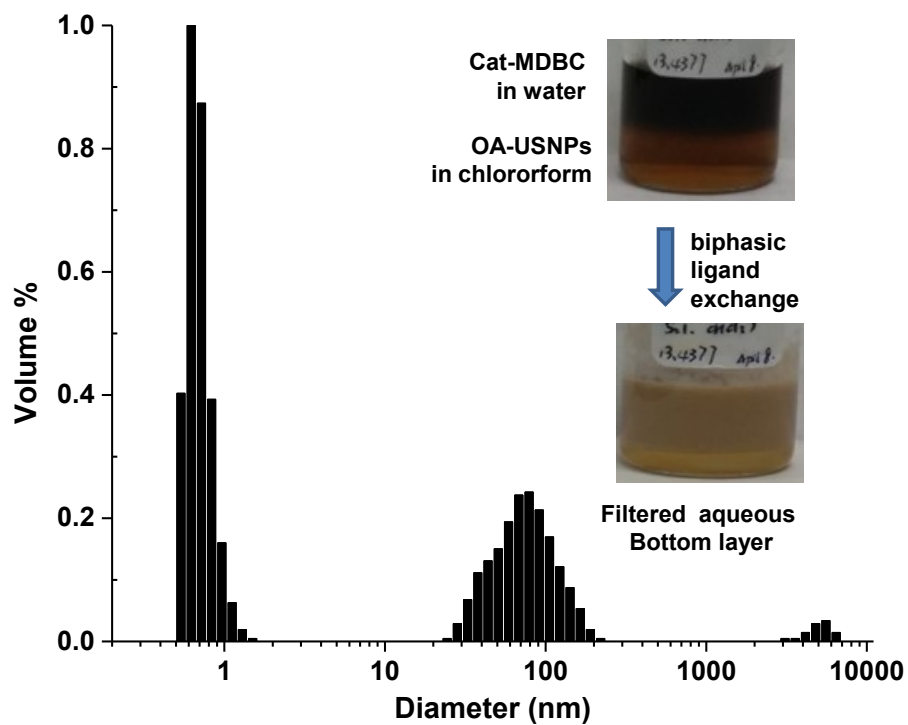
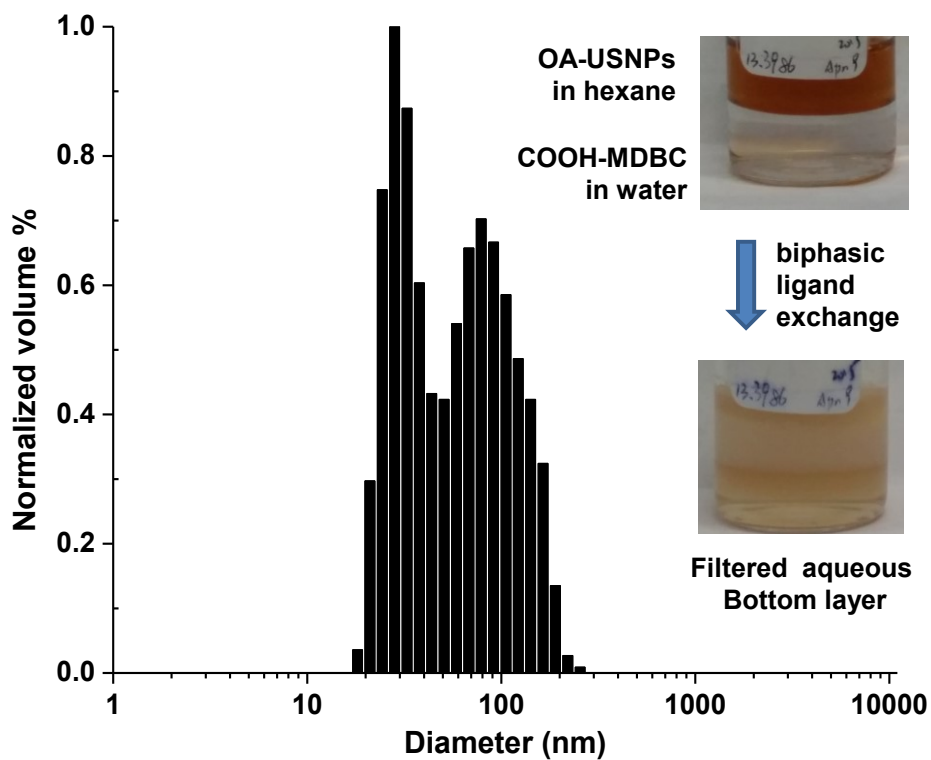
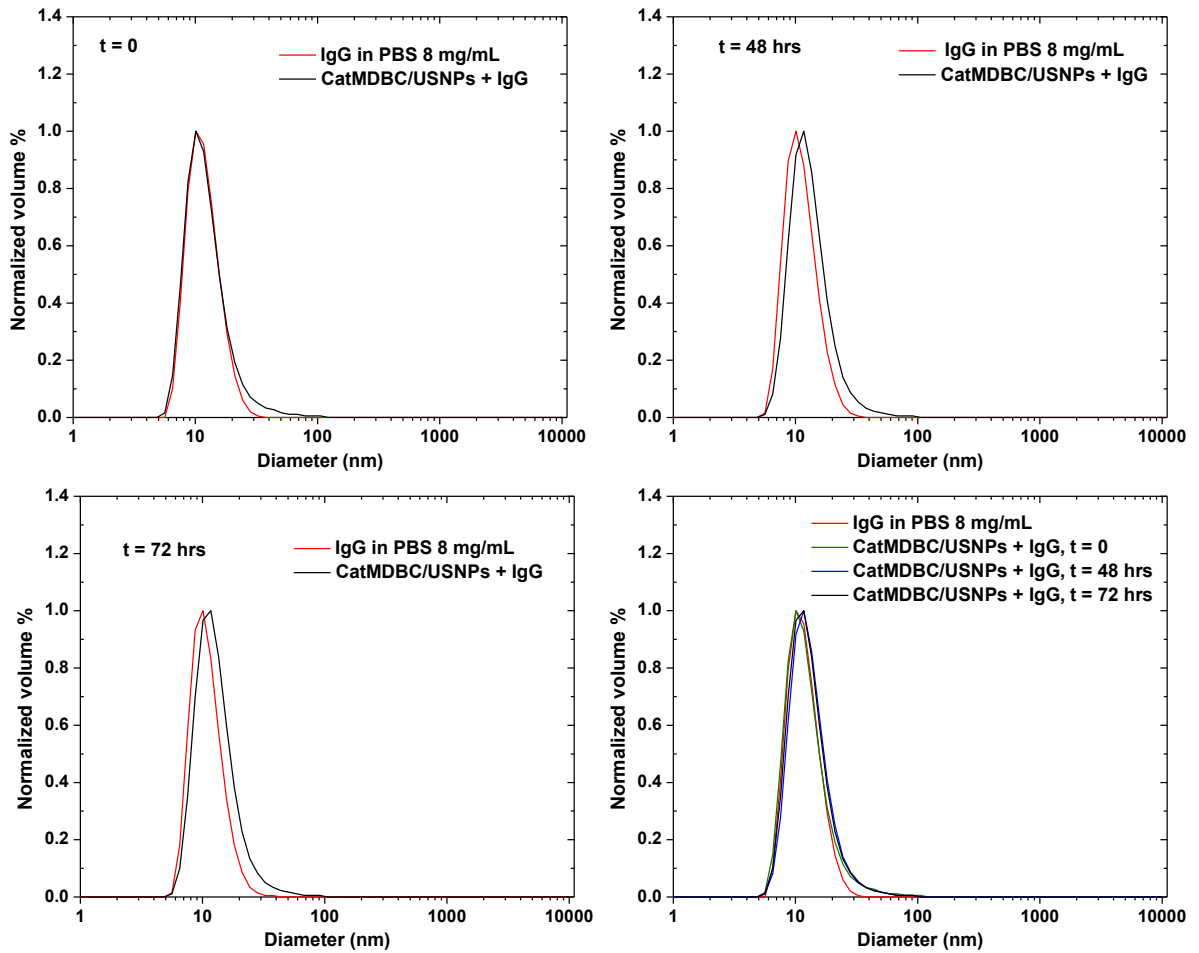


Figure A7. DLS diagram and digital image (inset) of COOH-MDBC/USNP colloids in water, prepared by biphasic ligand exchange process with hexane as an organic phase.



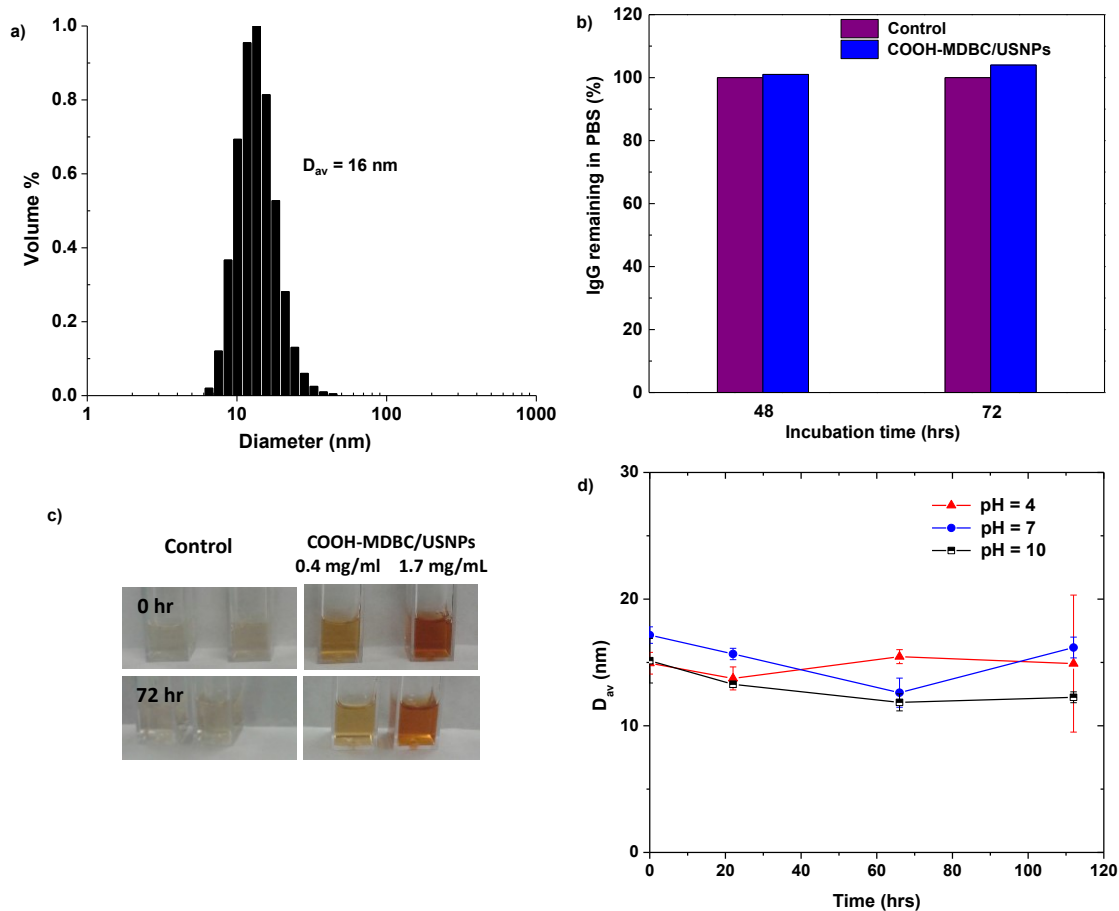
III) Colloidal stability

Figure A8. DLS diagrams of aqueous Cat-MDBC/USNP colloids incubated with IgG protein (8 mg/mL) for 48 and 72 hrs.



IV) Colloidal stability of COOH-MDBC/USNPs

Figure A9. For aqueous COOH-MDBC/USNP colloids prepared by conventional ligand exchange process, DLS diagram in aqueous solution (a), no significant interaction with IgG protein (8 mg/mL) over 72 hrs determined by BCA assay (b), digital images of their mixtures with human serum at 0.4 and 1.7 mg/mL (c), and evolution of their diameter over time at various pH = 4, 7, and 10 (d).



V) Synthesis and ligand exchange of Cat-MDRC

Figure A10. Synthetic route to Cat-MDRC (a) and $^1\text{H-NMR}$ spectra in DMSO-d_6 (b).

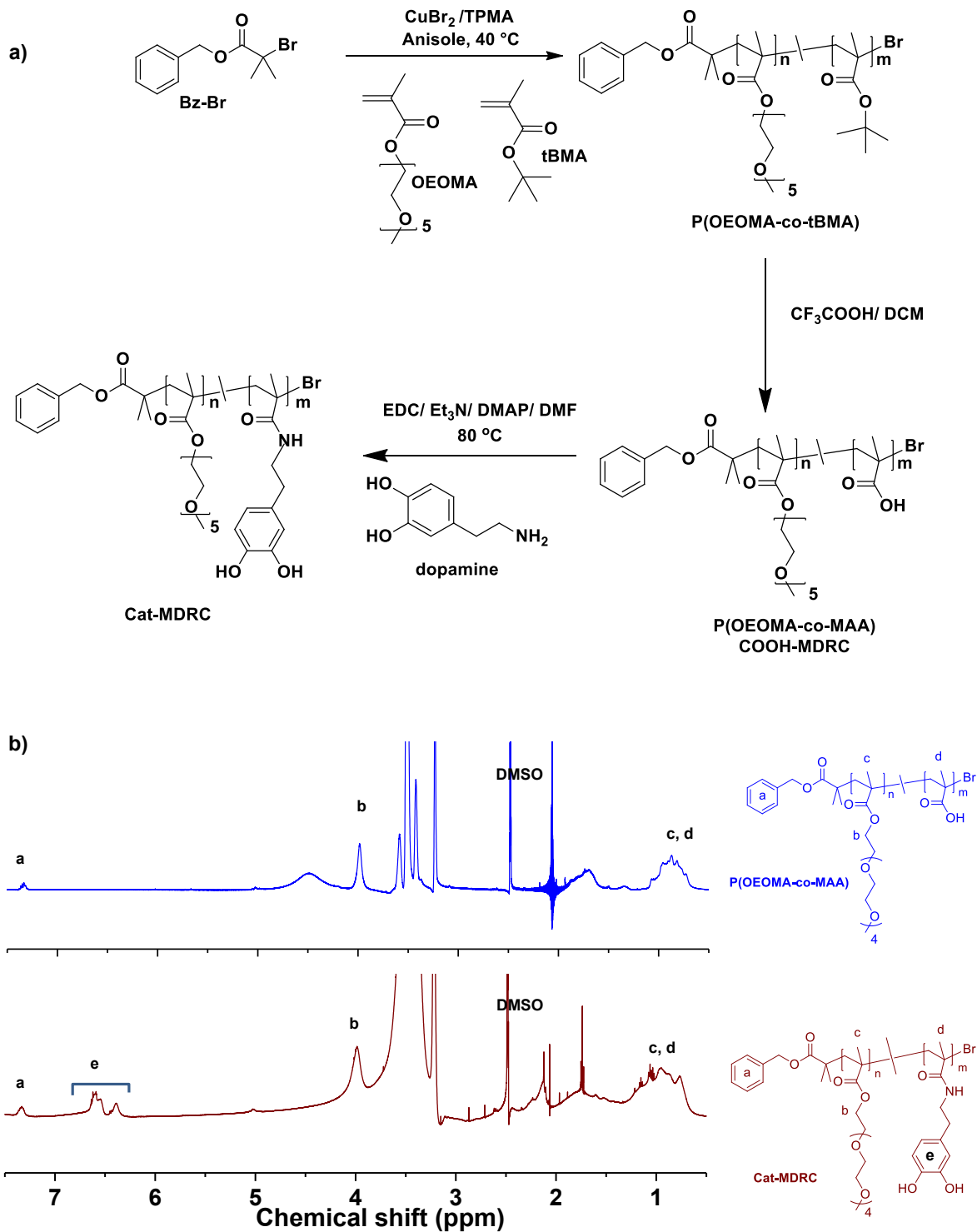
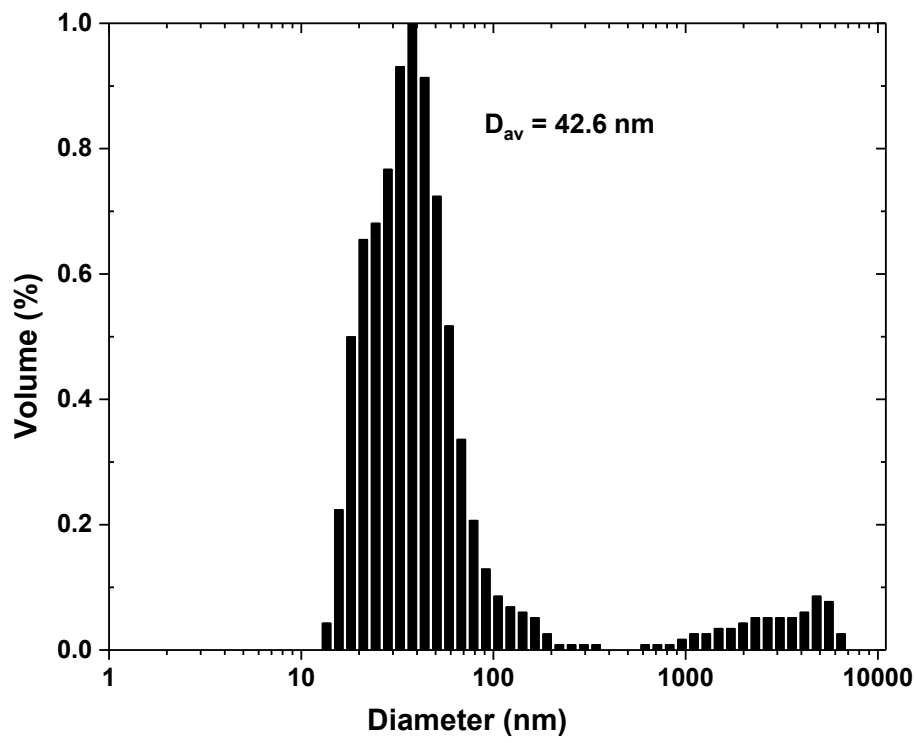


Figure A11. DLS diagram of Cat-MDRC/USNP colloids in water, prepared by conventional ligand exchange process.



Appendix B

I) Biphasic ligand exchange

Calculation of biphasic ligand exchange efficiency by ICP measurements

From ICP measurements, Fe = 18.4 ppm in 8.1 mL recovered water phase after biphasic ligand exchange. Thus, Fe = 0.149 mg. From the recipe, OA-ESNPs = 7.5 mg; Fe₃O₄ content in OA-ESNPs = 45.5% by TGA and Fe content in Fe₃O₄ = 72.4% by elemental calculation. Thus, Fe = 7.5 mg × 45.5% × 72.5% = 2.47 mg (assuming that all Fe₃O₄ NPs in hexane are transferred to aqueous phase during biphasic ligand exchange process). Thus, efficiency = 0.149 mg/2.47 mg × 100 = 6%.

Figure B1. TGA trace of Cat-MDBC/ESNP, compared with those of OA-ESNPs and Cat-MDBC.

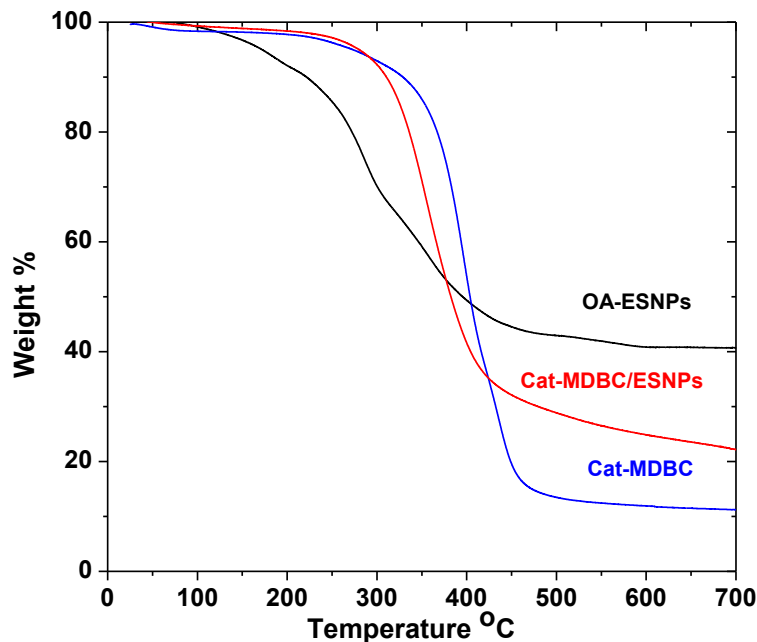


Table B1. Weight lose calculation based on TGA results

TGA	A	B	C	D	E
	Point 1 around 200 °C	Residual weight% at platform around 600 °C	Weight lose % A-B	Calibrated polymer weight lose% without H ₂ O(C/A)	weight lose% without H ₂ O and if all polymer burnt out D/88.1%
Cat-MDBC	96.3%	11.5%	84.8	88.1	
OA-ESNPs	89.6%	40.8%	48.8	54.5	
Cat-MDBC/ESNPs	97.2%	23.6%	73.6	75.7	85.9

II) Calculation of UV-Vis titration

Figure B2. UV-Vis spectroscopic monitoring during titration of dopamine hydrochloride using Fe^{3+} (a), Profiles of the absorbance at 570 nm with the addition of the Fe^{3+} into dopamine hydrochloride (b), Multivariate fitting yielded a binding constant $\log_{10}K = 6.343 \pm 0.048$ for 1:1 model (c,d).

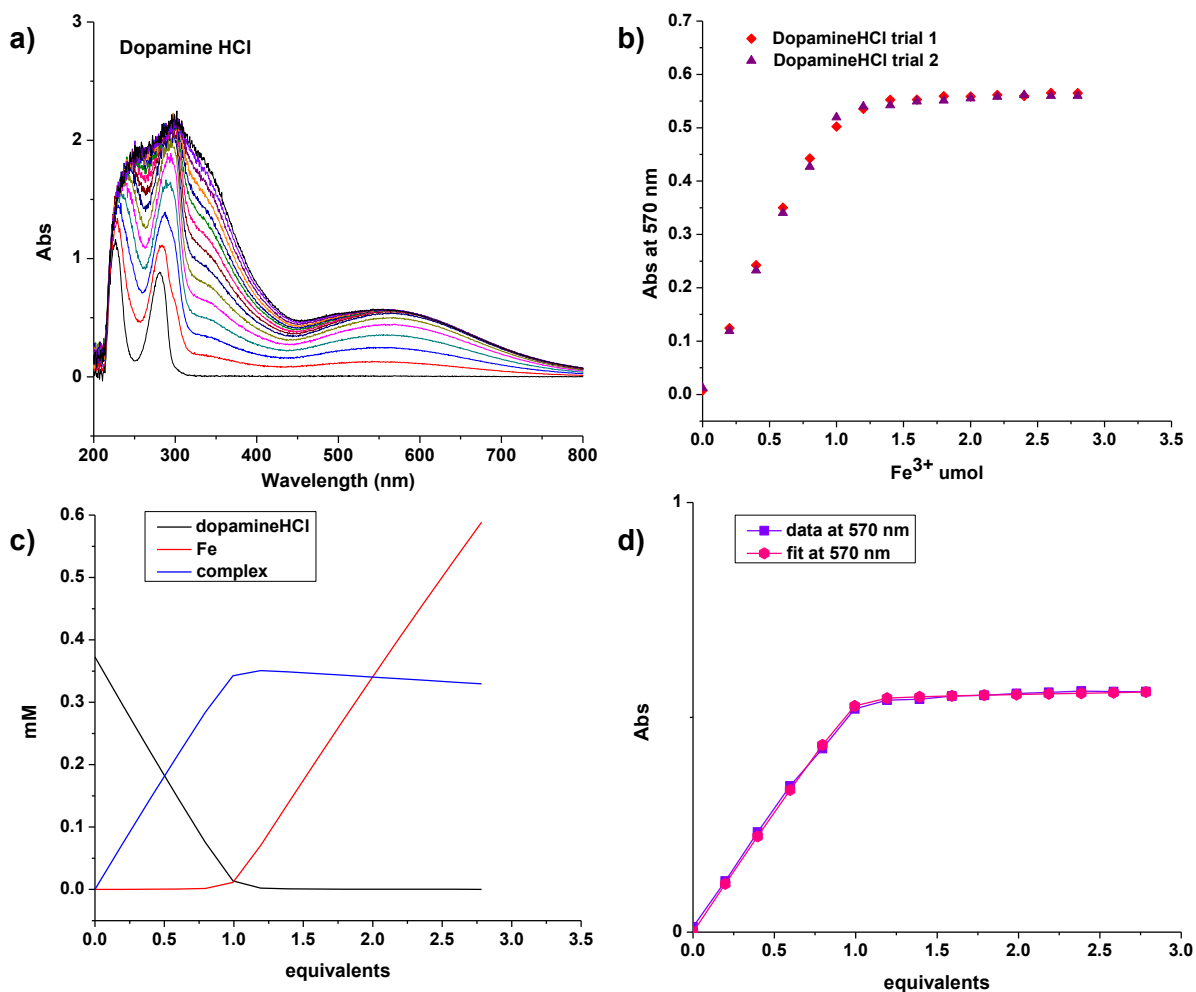
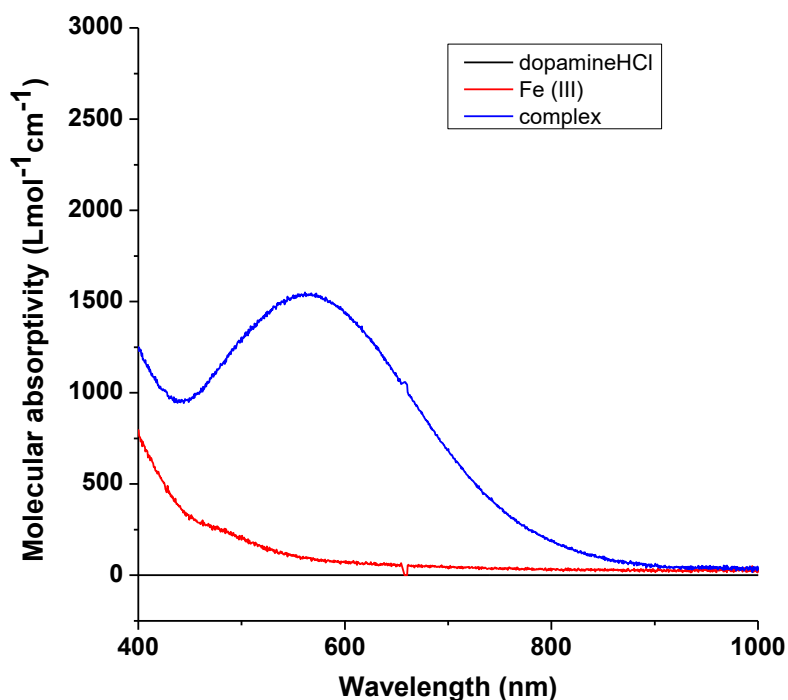
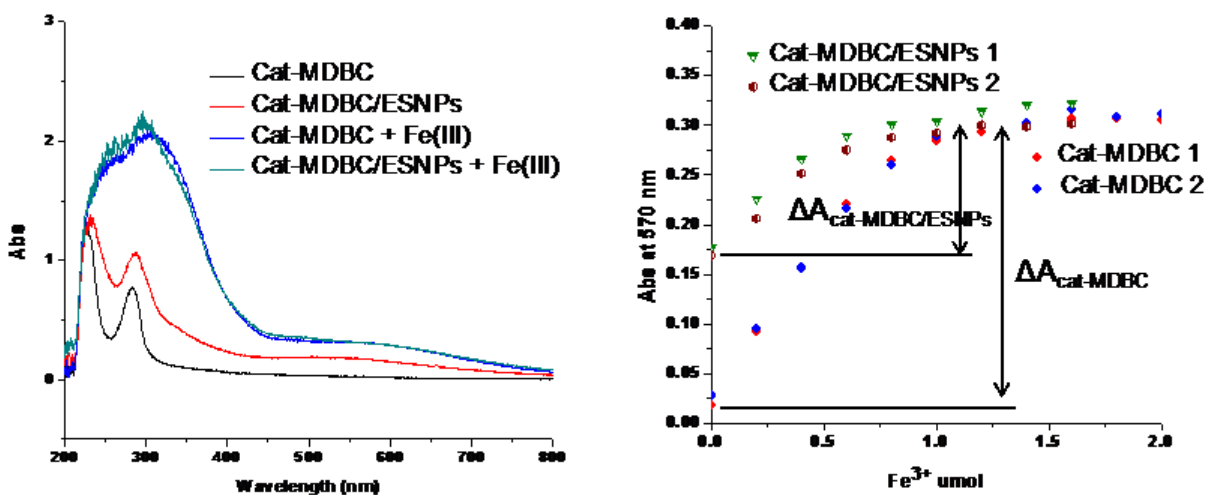


Figure B3. The molar absorptivities (ϵ in Beer-Lambert Law $A = \epsilon cl$) of Fe^{3+} , dopamineHCl their complex at different wavelength.



Calculation of percentage of unbound catechol groups based on UV-Vis titration:

Figure B4. UV-Vis spectra overlap of the Cat-MDBC and Cat-MDBC/ESNPs before and after titration (left). Overlap of the absorbances at 570 nm with the addition of the Fe^{3+} into Cat-MDBC and Cat-MDBC/ESNPs (right).



The first calculation method is based on the changes in Abs at 570 nm from starting point to the plateau during the titration ($\Delta A_{\text{Cat-MDBC}}$, $\Delta A_{\text{Cat-MDBC/ESNPs}}$ shown in Figure B4) as well as the linear fitting $\text{Abs} = \text{Slope} \times \text{Mole}_{\text{Fe}} + \text{intercept}$ obtained from the data point of Cat-MDBC titration before reaching the plateau. The linear fitting obtained from trial 1 and trial 2 were $\text{Abs} = 0.448 \text{ Mole}_{\text{Fe}} + 0.015$ and $\text{Abs} = 0.374 \text{ Mole}_{\text{Fe}} + 0.026$ respectively. $\Delta A_{\text{Cat-MDBC}} = 0.28 \pm 0.01$, so according to the linear fitting the corresponding $\Delta \text{Mole}_{\text{Fe}} = 0.625 \text{ mol}$ and 0.748 mol respectively and the average is 0.687 mol . Similarly, $\Delta A_{\text{Cat-MDBC/ESNPs}} = 0.14 \pm 0.01$ corresponding to $\Delta \text{Mole}_{\text{Fe}} = 0.313 \text{ mol}$ and 0.374 mol respectively and the average is 0.344 mol . Since under these titration condition, the equivalent of Fe^{3+} : catechol = 1:1, and the total amount of Cat-MDBC is designed to be same in UV-Vis titration of Cat-MDBC and Cat-MDBC/ESNPs so the percentage of unbound catechol groups in Cat-MDBC/ESNPs = $0.344/0.687 = 50\%$.

There is another approach to calculate the percentage of unbound catechol groups in Cat-MDBC/ESNPs based on $\Delta A_{\text{Cat-MDBC}} = 0.28 \pm 0.01$, $\Delta A_{\text{Cat-MDBC/ESNPs}} = 0.14 \pm 0.01$. According to Beer-Lambert Law $A = \epsilon cl$, in our experiment both light path l (1 cm) and ϵ_{570} are constant, therefore the concentration change (Δc) of Fe(III)-catechol complex from beginning to plateau equal to $\Delta A/(\epsilon l)$. In the previous titrations of dopamine hydrochloride, the equivalent of Fe^{3+} : catechol = 1:1, therefore the ΔA ratio = $0.14/0.28 = 50\%$ represents the percentage of unbound catechol groups in Cat-MDBC/ESNPs

List of Publications

P. Li, P. Chevallier, P. Ramrup, D. Biswas, D. Vuckovich, M.-A. Fortin, J. K. Oh.* Mussel-inspired multidentate block copolymer to stabilize ultrasmall superparamagnetic Fe₃O₄ for magnetic resonance imaging contrast enhancement and excellent colloidal stability, *Chemistry of Materials* **2015**, *27*, 7100-7109.

T. Sun, P. Li, J. K. Oh.* Dual location dual reduction and photo-responsive degradable block copolymer micelles: disassembly and synergistic release, *Macromolecular Rapid Communications* **2015**, *36*, 1742-1748. **(invited back cover)**

N. Chan, P. Li, J. K. Oh.* Chain length effect of multidentate block copolymer strategy to stabilize ultrasmall Fe₃O₄ nanoparticles, *ChemPlusChem* **2014**, *79*, 1342-1351. **(Nominated for a special edition entitled "Early Career Series")**